

## **Response to the referee comments on the manuscript:**

Title: Growth of ice particle mass and projected area during riming

By: Erfani, Ehsan; Mitchell, David

Article reference: acp-2016-455

We wish to thank the referees for their detailed and helpful comments on our paper. As you will see below we have responded to all of the comments with revisions designed to address the concerns of the referees. In the following response, the original referee comments appear in black and our responses appear in blue and are labeled “Author response:”

### **Referee comments:**

#### **Anonymous Referee #1:**

Review of “Growth of ice particle mass and projected area during riming” From Ehsan Erfani and David L. Mitchell

Overview:

The authors investigate the riming effects in frontal cloud systems in the Sierra Nevada, on coefficients of mass-size and area-size relationships. They used a dataset (referenced as SCPP in the paper) described in Mitchell et al. 1990 and also used in Mitchell (1996) and Baker and Lawson (2006) who are often cited in recent scientific studies. In the third section, SCPP dataset is compared to a recent mass-diameter fitted curve. This fitted m-d relation was developed with mass and diameter derived from CPI images using the area-mass relationships given in Baker and Lawson 2006, and a part of the SCPP dataset (call cold habit). CPI images represent ice particles for temperature colder than  $-20^{\circ}\text{C}$  in cirrus and anvil clouds during the aircraft measurement of the field campaign SPARTICUS. Ice particles of the SCPP dataset are divided in two parts: rimed and unrimed particles. Authors show that rimed particles are heavier than unrimed particles for a same size. Furthermore, ice particles of the SCPP dataset are stored by size bins where average mass are calculated and compared to the EM16 mass-diameter relationship, authors conclude that the EM16 fitted curve is representative of mass-size relationships of ice particles in clouds for temperatures between  $-40^{\circ}\text{C}$  and  $-20^{\circ}\text{C}$ . Section 4 is dedicated to the effects of riming on mass-size and area-size coefficients. In a first step the study is performed with heavily rimed and unrimed dendrites where mass-size relations are calculated for each type of dendrites. It is shown that heavily rimed dendrites have around twice the mass of unrimed dendrites in average and that power of m-d relations are similar for both types of dendrites: 1.78. Hence, authors found that riming process affects only  $\alpha$  in m-d power law and that increase of  $\alpha$  is a proxy to study the evolution of the riming process. Then a riming factor is defined as the ratio the mass of the ice crystal less its mass when it is unrimed divided by the difference between the mass of the ice crystal when it is a graupel and its mass when it is unrimed. Then weighted average ratios are calculated between unrimed dendrites and graupel and between hexagonal columns and graupel. Calculated ratios are: 3.3 and 2.4 respectively, which define the maximum mass of dendrites habit and columns habit such  $m_{\text{max}}=3.3 \cdot \mu$  ( $\mu$  for mass

of unrimed crystals) and  $m_{max}=2.4*\mu$ , respectively. In section 5 authors provide fits of collision efficiency between ice crystals such (columns and plates) and supercooled droplets using data of WJ00. The work is done for different Froude number and Stokes number. Others references are used to avoid discontinuities in different regimes. Section 6 is dedicated to the calculation of the mass growth rate due to the riming process. To do this, results of section 5 are used. The method is applied for hexagonal plates and a droplet size distributions following a Gamma function. Results obtained show that  $dm/dt$  for riming increase with  $D$  of plates. Furthermore, for a same Liquid water content doubling  $m_{md}$  from 8 to 16 microns leads to times by 4  $dm/dt$ . Note that a LWC of 0.05 g/m<sup>3</sup> with  $m_{md}$  of 16 microns gives  $dm/dt$  of the same order than for a LWC of 2g/m<sup>3</sup> and a  $m_{md}$  of 8microns. Increase  $m_{md}$  is more efficient than increase LWC.

General comments: The topic of this study could be very useful for experimental and numerical simulations studies about physical processes of ice hydrometeors in clouds. However, I find that this work is not finalized and it could be improved with further investigations. Also it does not meet the basic criteria of ACP: does the study “represent a substantial contribution to scientific progress within the scope of Atmospheric Chemistry and Physics (substantial new concepts, ideas, methods, or data)”

Author response: While it is not clear why this reviewer feels that this work is not finalized and not a “substantial contribution”, it should be mentioned that this is the 2<sup>nd</sup> paper in a three-part series that began with an extensive development of ice particle  $m$ - $D$  and  $A$ - $D$  relationships (now published in ACP; Erfani and Mitchell, 2016). The 3<sup>rd</sup> paper (soon to be submitted to ACPD) presents a new snow growth model (SGM) that predicts the steady-state height evolution of the ice particle size distribution (PSD) due to ice particle growth by vapor diffusion, riming and aggregation (as well as updraft effects on the PSD evolution). The riming treatment in this SGM is based on this 2<sup>nd</sup> paper, and the SGM is tested against the evolution of observed PSD in a deep mixed phase cloud. These three papers certainly constitute a “substantial contribution”, but the first ACP article alone is 22 pages, and to combine all these papers into a single article does not make sense as per normal journalistic standards. Combining the 2<sup>nd</sup> and 3<sup>rd</sup> papers would also result in an article of unacceptable length.

Another reason for limiting this paper to the development and description of a scheme for modeling the riming process is to present this scheme in a manner that will be general for use in most bulk microphysical parameterizations (BMPs). Most BMPs use  $m$ - $D$  and  $A$ - $D$  power laws to parameterize the microphysical processes, but no BMPs that we know of have represented these power laws as a function of riming. This representation is needed in BMPs to realistically treat the riming process, and this paper provides a means of doing this. Thus, we argue that a compelling need exists to improve BMPs in terms of the riming process, and that providing a general approach to address this need is indeed a “substantial contribution”.

Authors shows only results for one type of ice crystals habits that the power of  $m$ - $d$  stay constant during the riming. This result was already suggested in former studies which are cited in this study.

Author response: In addition to show the results for dendrites, we showed this for all ice particles in SCPP data with various shapes. Regarding the originality of our work: first we are aware of only one observational study (Rogers, 1974) that suggested the conservation of  $\beta$  for snowflakes

during the riming process. No other observational study investigated this result. Second, the modeling study of Morrison and Grabowski (2008; henceforth MG08), Morrison and Grabowski (2010) and Morrison and Milbrandt (2015) used the result of Rogers (1974) as a basis for their models. In addition, Morrison and Milbrandt (2015) also used Table 1 in Mitchell et al. 1990 (henceforth M90) for hexagonal columns and our preliminary results (from our conference paper: Mitchell and Erfani, 2014) for dendrites to support the assumption of constant  $\beta$  for their model. Only a very limited number of models utilized this method (constant  $\beta$  during phase 1 of riming), and we think that further investigation of this assumption by extra observations will be very useful for atmospheric modeling. Thus, our study is not a repetitive study. Finally, investigation of  $\beta$  during the riming was only a part of our study. One important achievement in our study is developing a method for growth of projected area, which is unprecedented. Previous studies were focused on mass and not projected area. In fact, MG08 mentioned the discontinuity in projected area that they observed in their model. Another important result of our study is the formulation of the cloud droplet-ice crystal collision efficiency for planar and columnar ice crystals, based on more recent numerical results from fluid-dynamic modeling studies. Such calculations were needed because the vast majority of cloud models use a collision efficiency formulation from an old study that is based on an older theoretical data with many limitations and assumptions. Therefore, we think that our numerically practical treatment of the riming process may be very significant in the field of atmospheric science and can be easily used in climate and cloud models.

Some results of the M90 dataset argue against the main results of this paper without being discussed. Also the M90 dataset is not appropriate to extend this kind of results for in-clouds habits conclusions, as it concerns only precipitated ice particles. Results should be take more carefully.

Author response: We would be happy to discuss any discrepancy between our results and M90 if such disagreement was mentioned explicitly.

M90 dataset is a unique available dataset that measures both ice particle size and mass, as well as the degree of riming, for many ice particle shapes. Aircraft do not provide such measurements, and there is no other dataset that we know of having these attributes and that suits our purpose. Cloud base was not far from the sample collection site, and sublimation effects were not evident based on crystal shapes. As explained in Erfani & Mitchell (2016, ACP; henceforth EM16), the important problem with airborne measurements is that they are unable to measure single ice particle mass. Nonetheless, we compare our results with m-D relationships from previous studies (Heymsfield et al., 2010; Cotton et al., 2012; EM16) that are based on airborne measurements.

We added this explanation to Data and Method, page 9, starting at line 5:

“SCPP is a unique dataset that measures both ice particle size and mass and also determines the degree of riming. As explained in EM16, the important problem with airborne measurements is that they are unable to measure single ice particle mass. Nonetheless, we compare our results with m-D relationships from previous studies (Heymsfield et al., 2010; Cotton et al., 2012; EM16) that are based on airborne measurements.”

Section on area-size relationships should be strongly reconsidered as it based on no new experiments or numerical simulation data, there is only a discussion about older results which brings no new results. I recommend to rewrite this paper by keeping section five and developing section 6 for not only hexagonal plates but also hexagonal columns and dendrites habits (has

these habits are used in this paper) while section 4 could be used to compare numerical results of section 6. Mass growth rate could be compared to the mass of unrimed ice crystals as a function of  $D$ , to confirm or not the experimental results who shows that power of  $m$ - $D$  relation is constant during the riming process until the graupel formation.

Author response: The use of a measurement database in other studies does not disqualify its use in new studies if the new study has found a unique purpose for the database. It is possible that this SCPP database has been used in other studies due to its uniqueness (these measurements are extremely labor-intensive) and the utility of these single-particle measurements. Our study has found a new application for this SCPP database; the treatment of  $m$ - $D$  and  $A$ - $D$  relationships as a function of the riming process as described in Sect. 4.

Although Sect. 4.2. on the effect of riming on projected area has some limitations (and we mentioned the limitations at the beginning of this section), we think this section is a new theoretical approach that is important for these reasons: MG08 used different  $A$ - $D$  power laws in each riming step, but such method led to discontinuities in projected area during the transition from one ice category to another one. It seems that the  $A$ - $D$  and  $m$ - $D$  that they used were not self-consistent (e.g. they were from different studies based on different datasets). We understand this challenge to find self-consistent  $m$ - $D$  and  $A$ - $D$  expressions, and as we mentioned, there are no projected area-dimensional measurements in SCPP data. Therefore, we conclude that by calculating area from mass (as described by Eqns. 10 & 11) there will be no discontinuity in area. We used the results of previous studies (such as Fontaine et al., 2014; Heymsfield 1978; Jensen & Harrington, 2015; henceforth JH15) to develop our riming formulation. Our formulation is a new development, and it is not a mere repackaging of previous findings. In addition, we use this approach in our future paper (Erfani et al., 2017) and show how it improves the simulation of projected area during the riming process. We added this explanation at the beginning of Sect. 4.2:

“MG08 used different  $A$ - $D$  power laws in each riming step, but this method led to discontinuities in projected area during the transition from one ice category to another one. It seems that the  $A$ - $D$  and  $m$ - $D$  that they used were not self-consistent (e.g. they were from different studies based on different datasets). Here, we suggest an approach to avoid the discontinuity in projected area.”

Regarding the development of Sect. 6, we added an extra panel in Fig. 6 to show the mass growth rate for hexagonal columns (Fig. 6.b), along with explanations in the text. It is not feasible for us to extend the research for dendrites, because it strongly depends on the derivation of collision efficiency for dendrites, which has not been done for this study and it needs extra time and resources which is not possible for us to do at this time. The explanations for hexagonal columns mass growth rate have been added to the manuscript at the end of the second-to-last paragraph in Sect.6:

“One important feature is the contribution of small droplets ( $d < 10 \mu\text{m}$ ) to  $dm/dt$ , when  $K < 0.7$  and  $E_c < 0.3$ . It is seen in this figure that when MMD is relatively small ( $= 8 \mu\text{m}$ ), ignoring such small droplets results in values of  $(dm/dt)_{riming}$  at the largest crystal sizes that are  $\sim 40\%$  (for plates) and  $\sim 70\%$  (for columns) of those obtained when all droplets are included. That is, small droplets contribute about 60% and 30%, respectively, to the  $(dm/dt)_{riming}$  values at the largest sizes. This surprising contribution from small droplets is partly due to half of the LWC being associated with  $d < 8 \mu\text{m}$ . However, when MMD is larger ( $= 16 \mu\text{m}$ ), the contribution from small droplets is only  $\sim 5\%$ . The size-dependence of  $dm/dt$  for hexagonal columns (Fig. 6b) shows that

$dm/dt$  for columns is larger than that for hexagonal plates for a specific crystal size when droplet MMD is 8  $\mu\text{m}$ , partly because columns fall faster than plates (see Fig. 6 in M96) and partly due to higher  $E_c$  for columns encountering larger droplets. Moreover, when LWC is constant, doubling MMD (from 8 to 16  $\mu\text{m}$ ) leads to at least a doubling of  $dm/dt$  (greater for plates).”

Regarding the calculation of mass growth rate for unrimed ice crystals, it needs to calculate mass growth rate for microphysical processes other than riming (e.g. vapor deposition and aggregation), which is beyond the scope of this study. However, our snow growth model (SGM), which is the subject our future paper (Erfani et al., 2017) includes three growth processes of vapor deposition, aggregation, and riming, and your question in this regard will be answered in our future paper. This is reflected at the end of conclusions, page 25, starting at line 28:

“... In the future, this treatment of the riming process will be employed in a new SGM that predicts the vertical evolution of ice particle size spectra, mass, projected area, fallspeed, and snowfall rate in terms of the growth processes of vapor diffusion, aggregation and riming. These results will be compared with airborne measurements from two spiral descents.”

Moreover, it could be extended to a theoretical/numerical study on the riming factors as a function of time which could be useful for future studies with ground radar observations versus aircraft measurement. To finish this study could compare numerical results with experimental data as SPARTICUS and SCPP datasets.

Author response: This is the subject of another paper that we are preparing (Erfani et al., 2017). We developed a snow growth model (SGM) to simulate microphysical processes of vapor deposition, aggregation and riming. In addition, aircraft data from two Lagrangian spiral descents are used to compare the model with observations.

Specific comments:

P8, lines 3-5: what kind of modification, is it possible to resume with few words?

Author response: We added these explanations in this part of manuscript for clarification:

“Similar to Beard and Grover (1974), they employed the superposition method for collision between particles, but they assumed that the small cloud droplets do not change the graupel fallspeed. Therefore they used the Stokes number instead of the mixed Froude number in the non-dimensionalized momentum equation (see Eqs. 1-6 in Rasmussen and Heymsfield, 1985).”

P9, line 2: As the riming is the purpose of the paper. I suggest a figure with few examples of microprobe images to show each riming level of ice crystals who are studied.

Author response: Since the high-magnification photos taken during SCPP do not contain examples of rimed ice crystals corresponding to these 4 riming levels, we cite the Magono and Lee ice particle classification scheme that was used to classify ice particle shape during SCPP. The 4 riming levels used come from the Magono and Lee scheme, which provides illustrations for each ice particle type. The following text was added: “Also recorded were individual ice particle shapes, which were classified using the Magono and Lee (1966) nomenclature scheme. The level of riming (i.e. light, moderate, heavy riming, or graupel) was indicated based on this scheme, and the temperature range over which the observed ice particle shape originated was recorded (e.g. for long columns,  $-8^\circ\text{C} < T < -6^\circ\text{C}$ ). These riming levels are indicated (with rimed

crystal illustrations) in the Magono and Lee (1966) ice particle classification scheme with the prefix R1, R2, R3 and R4 (see Pruppacher and Klett, 1997, p. 46). Photographic examples of these rimed particle types are shown in Fig. 2 of Locatelli and Hobbs (1974).”

P9, line 3: is it the ground temperature, or temperature are deduced using diagram (for example Pruppacher and Klett 1997; Magono and Lee 1966; Bailey and Hallet 2009), then few explanations are expected.

Author response: The latter is used. This has been clarified in the above paragraph that was added to the manuscript.

P9, line 6 (P10, line 10): CPI images doesn't give the mass of Ice crystals. Which approximation did you use to deduce the mass of ice crystals from CPI images?

Author response:

Appendix B in Erfani and Mitchell (2016) explained the method to approximate CPI mass. In the first paragraph of this Appendix B it is written: "There is no direct measurement of ice particle mass by the CPI probe. Moreover, the Baker and Lawson (2006) m-A relationship is based on ice particles larger than 150  $\mu\text{m}$ . Therefore, we developed a new method for estimating mass based on CPI measurements of ice particle projected area, length and width. It is assumed that when  $10 \mu\text{m} < D < 100 \mu\text{m}$ , all ice crystals are hexagonal columns. The apparent aspect ratio, defined as the CPI measured mean length-to-width ratio for a given size interval, is generally between 1 and 2 in this size range and the ice crystals are known to be relatively dense (more mass per maximum dimension), making this shape assumption a reasonable approximation (Korolev and Isaac, 2003; Lawson et al., 2006). This is more accurate than assuming ice particles to be spherical."

A brief explanation has been added to this part of the manuscript:

“Since CPI does not measure ice particle mass, EM16 developed a method that calculates mass from the measurements of ice particle projected area, maximum dimension, and aspect ratio by assuming that small ice particles can be approximated as hexagonal columns (for more details, see Appendix B in EM16).”

P 11, lines 6-11: Is there rimed particles in the cold habit and SPARTICUS fit? Or do you know if the ratio of rimed/unrimed particles are the same for both datasets in the comparison? If the ratio of unrimed and rimed particles are not equivalent, does it mean that the fit curve is representative of ice clouds between 40°C and -20°C. “To summarize, it appears .... A realistic bulk estimates for ice particle masses in frontal clouds.” A part of SCPP dataset is used to fit the curve of cold habit? Then what is the ratio of the SCPP dataset compared to SPARTICUS dataset in this curve fit? Because the conclusion is not surprising if the rate of SCPP dataset is significant compared to SPARTICUS dataset.

Author response: This section was not well written and apparently produced some confusion. The writing of this section has been improved, especially the first sentence: “The purpose of this section is to demonstrate how the cold habit SCPP curve fit from EM16 (based on unrimed ice crystals) compares with all the SCPP data, since this shows how the EM16 curve fit appears representative for all ice particles sampled during SCPP and thus may be representative for Sierra Nevada snowfall.”

As stated in Sec. 2, there are 827 ice particles in the cold habit (EM16) SCPP dataset and there are 4869 ice particles in the total SCPP dataset.

P13, lines 3-4: Watching the same table1 in M90, I can see that it is not true for needles and rimed needles. So it seems that it is not true for all ice crystals habit.

Author response: Yes, while this is true, only 7 rimed needles were sampled in M90 ( $\beta = 2.1$ ) and only 16 unrimed needles were sampled ( $\beta = 1.8$ ; same as for unrimed and rimed columns). Thus, the statistics are too poor to say much about  $\beta$  for rimed needles. We mentioned rimed and unrimed hex columns since these have relatively good statistics and are graphically displayed and analyzed in Sec. 4d of M90, along with aggregates of rimed and unrimed hex columns (which also support our evidence of constant  $\beta$  during riming).

P14, lines 4-15: there is missing in your statistical analysis, the both dataset that you conclude are identical should have an equivalent ratio of rimed and unrimed ice particles. Especially if you want generalize your conclusions to all frontal clouds.

Author response: We used the same dataset (SCPP) that contains both rimed and unrimed particles. In order to be realistic, we did not change the ratio of rimed to unrimed ice particles, and instead we used the measurements with the observed ratio.

P15-P16: Definition of  $m_{max}$  and  $\alpha_{max}$ .  $m_{max}$  define the mass of one ice crystal when it can be considered as a graupel, as  $\beta$  is constant during the riming so  $\alpha$  increase until  $m=m_{max}$ . After what you define a riming factor such  $R=(m-\mu)/(m_{max}-\mu)$ . By looking the figure below, we can guess that  $m_{max}$  ( $\alpha_{max}$ ) is a function of  $D$ , as  $R$ . Maybe more investigations should be necessary (and/or maybe an application on the SPARTICUS dataset, or another dataset) to use  $R$  factors and understand how it quantify riming in clouds.

Author response: Riming does not occur for broad-branched crystals with  $D$  less than 200  $\mu\text{m}$  (Wang and Ji, 2000; this is also mentioned in the paper). Therefore, the extrapolation of the curves to  $D < 200 \mu\text{m}$  is not physically-meaningful. In addition, the data size range should be taken into consideration. The mean-bin size in SCPP data does not exceed 3500  $\mu\text{m}$ , and any extrapolation larger than this size should be taken with caution. In fact, we showed in the paper that the uncertainty for the largest size bin is higher for unrimed dendrites, and it might be safe to use the second largest size bin ( $D = 2800 \mu\text{m}$ ) as the upper range.

Based on Figs. 3 and 4 in our manuscript, we do not see any meaningful relationship between the mass ratio and  $D$  in SCPP data. There is no riming information in SPARTICUS data, so we cannot use it for this purpose. Therefore we cannot make any conclusion or guess about the dependence of mass ratio on  $D$ . Indeed, Figs. 3 and 4 suggest that there is no such dependency.

P17, lines 16-22: I think that BL06 study is also performed on the SCPP dataset!?

Author response: As explained in Erfani and Mitchell (2016), BL06 used a subset of ice particles (865 particles) measured during SCPP. Using image analysis software, the projected area of ice particles in this subset was calculated from their photographed magnified images. The BL2006 study found that ice particle projected area was a more reliable predictor of particle mass than was maximum dimension. Their  $m$ - $A$  power law was derived from many types of ice particle habits or shapes; of the 550 identifiable ice particles, 36% were moderately or heavily rimed.

This  $m$ - $A$  power law is now commonly used to estimate size-resolved mass concentrations from 2D-S probe measurements of projected area. Since BL06 used only a subset of the SCPP data to produce a  $m$ - $A$  relationship (not a  $m$ - $D$  relationship), comparison of their work and our study is meaningful.

This explanation has been added to this paragraph:

“BL06 used a subset of SCPP data (e.g. 865 ice particles), of which 550 were identifiable, and 36% of such identifiable particles were moderately or heavily rimed. They then developed a software to calculate ice particle projected area from their magnified images. Thereafter, they calculated a  $m$ - $A$  power law expression. Since BL06 used only a subset of the SCPP data to produce a  $m$ - $A$  relationship (i.e. not a  $m$ - $D$  relationship), comparison of their work and our study is meaningful.”

Technical corrections: Missing references for: P3, 16: Feng and Chang (1982) P4, 17: Fukuta and Takahashi (1999) P8, 16: Blohn et al. (2009) P9, 117: Magono and Lee (1966) P17, 18-19: Baker and Lawson (2006)

Author response: All the missing references have been added to the list. There is no Feng and Chang (1982) in the manuscript, instead the reference for Feng and Grant (1982) is added. The reference for von Blohn et al. (2009) has been in the reference list (number 3 from the end).

P23, line 1-14: a reference to Heymsfield and Westbrook 2010 is recommended. They also worked on the terminal velocities of ice crystals and improved Mitchell 1996 theory.

Author response: We added this reference and explanations to this part of manuscript. Now, the manuscript reads (starting at P23, L14, in original manuscript):

“In addition, Heymsfield and Westbrook (2010) developed an alternative method to improve M96 method, and calculated  $X$  as a function of  $m/A_r$  ratio, where  $A_r$  is area ratio (defined as the ratio of ice particle projected area to the projected area of a circumscribed circle around the particle; see Eq. 15 in Erfani and Mitchell, 2016).”

Figures: Figure1a: mathematical Formula could be a plus. A curve fit for rimed and unrimed particle should be added.

Author response: The mathematical formula for polynomial curve fit of CPI and cold-habit SCPP is added to this figure. The main message of this figure is to show how the SCPP data conforms to various  $m$ - $D$  expressions from literature. The rimed and unrimed curve fits overlap with the current  $m$ - $D$  expressions, and prevent to convey the message of this figure. Instead, we added the rimed and unrimed curve fits to Fig. 2

Figure2: I recommend a plot of curves fit of rimed, unrimed dendrites and graupel.

Author response: The  $m$ - $D$  power laws for unrimed and rimed dendrites and graupel have been added to this figure.

Figure 1 and 2: green curve and points are not visible enough.

Author response: We understand that green might not be as sharp as black, blue, and red, but we already used these colors as points or curve. If we use colors other than green or yellow, it will be very similar to blue, red, or their combination, and it will not be easy to distinguish between them and the red, blue or black curves or points. In addition, we will provide figures with higher resolution for publication, and that should decrease the problem.

P6, line 9: ice particle shapes are function of temperature and relative humidity (see Pruppacher and Klett 1997; Magono and Lee 1966; Bailey and Hallet 2009)

Author response: This sentence has been changed and the relative humidity dependency has been added.

P3, line 20: “ $M_f = \text{IWC times } V_m$ ”?

Author response: The multiplication sign has been added: “ $M_f = \text{IWC} \times V_m$ ”

P3, line 14: NWS is not defined.

Author response: The definition of NWS (National Weather Service) has been added.

## **Anonymous Referee #2:**

This paper provides a way to evolve m-D and A-D relationships during riming with the goal of being able to improve riming in models that rely on these m-D and A-D parameterizations for different ice categories. The authors use their own previous data fit to compare with observations from the Sierra Cooperative Pilot Project. They show that riming increases the mass of ice and argue that this increase in mass can be parameterized without changing the beta coefficient in the m-D relationships. They also provide collection efficiency parameterizations for both planar and columnar ice based on numerical calculations. While the goal of this paper is to improve models by using observations, this paper has major issues that need addressed before it can be published.

### Major issues:

Perhaps be more specific about how to use this method to improve models that rely on different ice categories. It seemed hard to follow just how and when rimed snow would become spherical or hexagonal graupel using this framework. By assuming graupel forms when the mass of ice has increased approximately three fold, assumptions about the type of graupel and its density are being made and this should be clarified.

### Author response:

In order for models with multiple ice categories to use our method, they should add two transitional phases during riming growth. Phase 1 simulates the growth of an ice crystal from unrimed crystal up to the graupel onset. In this phase, mass and projected area gradually increase, but size is unchanged. Phase 2 represents graupel growth. In this phase, the shape is unchanged, but mass, projected area, and size gradually increase.

We used lump graupel and cone-like graupel (R4b and R4c) from SCPP dataset to determine the rimed-to-unrimed mass ratio for hexagonal columns. These same graupel shapes with the addition of hexagonal graupel (R4a) are used to calculate this ratio for hexagonal plates. These are explained in Sect. 4. Since there is no information on particle density in SCPP data, we did not make any assumption on the graupel density. However, SCPP observations show the conservation of  $D$  and  $\beta$  during the phase 1 of riming, and since the initial graupel mass is  $\sim 3$  times larger than unrimed crystal mass, these mean that initial graupel density is  $\sim 3$  times larger than unrimed crystals. Ice particle density generally implies spherical geometry, making the concept somewhat artificial for non-spherical ice particles. Nonetheless, one can easily calculate the density from the m-D relationship, defining spherical volume with  $D$ .

The explanations on the application of our method to models have been added as a new paragraph to Conclusions, page 25, starting at line 23:

“It is straightforward for models with multiple ice categories to utilize our new method. This can be done by describing riming growth as two phases and removing the autoconversion process. Phase 1 simulates the growth from ice crystal to the onset of graupel formation. In this phase, mass and projected area gradually increase, but size is unchanged (Eqs. 6-11). Phase 2 represents

graupel growth. In this phase, the shape is unchanged, but mass, projected area, and size gradually increase (Eqs. 12-14).”

And the explanation on the assumptions for graupel shape and density is added to Sect. 4.2.1, page 15, starting at line 14:

“In order to determine  $m_{\max}$ , we calculated the  $m_r/m_u$  that corresponds to graupel (R4a, R4b, and R4c) and unrimed dendrites (P1d, P1e, and P1f), as shown in Fig. 4a. Small variability is seen for  $D < 1200 \mu\text{m}$  (ranges from 3 to 3.8, with the exception of smallest size bin), whereas large variability exists (between 1.6 and 8.4) for larger sizes due to the small number of graupel in each size bin. The weighted average for this  $m_r/m_u$  ratio is equal to 3.3 which can be used to estimate  $m_{\max}$ :  $m_{\max} \approx 3.3 \times m_u$  for the dendrites. Since R4a occurs just before hexagonal features are completely obscured by additional rime deposits, R4a graupel is ideal for estimating  $m_{\max}$ . Unfortunately, there are only 14 R4a particles in the entire SCPP data, with  $D < 1200 \mu\text{m}$ . They exhibit a large variability in the  $m_r/m_u$  ratio (ranging from 1.6 to 4.5) with a weighted average of  $m_r/m_u$  equal to 3.1 (figure not shown). Nonetheless the close agreement with the above  $m_r/m_u$  ratio of 3.3 is encouraging for us to conclude that initial graupel mass (at the end of phase 1) is 3.3 times larger than unrimed dendrites. Since the SCPP observations show that  $D$  and  $\beta$  are conserved during the first phase of riming, graupel density is also  $\sim 3.3$  times larger than unrimed dendrite mass.”

Perhaps the introduction needs an extra section on the treatment of riming in models after talking about the characteristics of riming. Also, perhaps the riming rate equation needs to be introduced (at least qualitatively) in the introduction before talking about riming and collection efficiencies.

Author response: We added an extra section (now: 1.2. treatment of riming in models) in the Introduction after the characteristics of riming and before the collision efficiency. We moved a paragraph on modeling of the riming (previously at the end of Sect. 1.1) to this section. We also added more explanations on the method of MG08. Moreover, an explanation on riming mass growth rate is added to this new section:

### “1.2. Treatment of Riming in Models

Since explicit modeling of the riming process is computationally expensive, graupel and hail categories were not considered in some bulk microphysics parameterizations used in some global climate models or GCMs (Morrison and Gettelman, 2008; Gettelman and Morrison, 2015). The common ice microphysics approach in most cloud and climate models is the separation of ice into various hydrometeor categories such as cloud ice, snowflakes, and graupel (Rutledge and Hobbs, 1984; Ferrier, 1994; Fowler et al., 1996; Reisin et al. 1996; Morrison and Gettelman, 2008; Gettelman and Morrison, 2015). The transition between various hydrometeors occurs by autoconversion from one hydrometeor category to another. However, such autoconversion is arbitrary and poorly constrained, and as shown by Eidhammer et al. (2014), cloud radiative properties were sensitive to the choice of autoconversion threshold size in the Community Atmosphere Model version 5 (CAM5). This is because the distinct boundaries between various ice hydrometeor categories impose abrupt changes in microphysical properties (such as ice

particle mass, projected area, fallspeed, and effective diameter) from one hydrometeor category to another, while in nature the transition processes are gradual.

To overcome this problem, MG08 advanced a bulk model that employed vapor diffusion and the riming processes, and used multiple  $m$ - $D$  and  $A$ - $D$  power laws (Eqs. 1 and 2) to characterize ice particles associated with different parts of the PSD. This method was applied to a bin model developed by Morrison and Grabowski (2010), and was later used in a bulk model that prognoses number concentration, rime volume, rime mass and total mass (Morrison and Milbrandt, 2015). In this approach, different  $m$ - $D$  and  $A$ - $D$  expressions from the literature are used for either pure ice crystals or graupel. Then,  $m$  and  $A$  are calculated in a transitional step as a function of  $D$  and rimed mass fraction. Such  $m$ - $D$  and  $A$ - $D$  expressions resulted in a gradual transition from crystal mass to graupel mass. However, discontinuities were observed in transition between various  $A$ - $D$  expressions over the PSD because the size range for each microphysical step (ice crystal, graupel, and transition) was calculated in a way to provide only continuous mass, and thus produced discontinuities in projected area. JH15 developed a detailed ice growth model that simulates ice particle habit and mass via the processes of vapor deposition and riming. This model is also a single-category scheme, but it does not employ  $m$ - $D$  and  $A$ - $D$  power laws; instead, it computes the growth of ice particles along the major and minor axes of oblate or prolate spheroids (representing hexagonal plates or columns). Therefore, the model is able to simulate simple ice particle shapes, and also captures the temperature-dependency of vapor deposition and the riming processes (since particle shape is a function of temperature and relative humidity; Magono and Lee 1966; Pruppacher and Klett 1997). The simulated ice particle shape, mass, and fallspeed are in good agreement with observational data from wind tunnel experiments on ice crystal growth.

The computation of rime mass (an increase in ice particle mass by riming) in models is performed by calculating the accretional mass growth rate (Heymsfield, 1982; Mitchell, 1995; JH15). When an ice particle falls in a cloud of supercooled cloud droplets, the increase in its mass due to accretion depends on ice particle features (e.g. fallspeed and projected area), droplet characteristics (e.g. mass and number concentration of droplets), and the collision efficiency ( $E_c$ ) between an ice particle and droplet. More details on mass growth rates are provided in Sect. 6, and  $E_c$  is described in the next section.”

$m$ - $D$  relationships are parameterizations which reduce the dimensionality of complex ice shapes. More discussion is needed on alpha and beta and what they mean. Alpha can be considered to contain density and thickness information, thus certainly it can contain all the change to  $m$ - $D$  during riming, but others could argue that because shape changes during riming beta should change at some point.

Author response:

We added extra sentences to explain the importance of  $m$ - $D$  relationships and to define  $\alpha$  and  $\beta$ . Erfani and Mitchell (2016) explained  $m$ - $D$  and  $A$ - $D$  relationships with more details. Regarding the change in  $\beta$ , we explain that with more details in the next comment.  $\beta$  starts to change at the beginning of phase 2 of riming, where ice particle has become graupel and has a quasi-spherical

shape. The explanations on  $m$ - $D$  expressions are added to manuscript, page 4, starting from line 21:

“Many models calculated ice particle mass by assuming that ice particles are spherical (e.g.  $m = \rho_i \pi D^3 / 6$ , where  $\rho_i$  is ice density; Rutledge and Hobbs, 1984; Ferrier, 1994; Morrison and Gettelman, 2008). However, this assumption is not realistic, and produces errors in the evolution of snow-size spectra (Mitchell, 1988). Based on observations, several studies developed ice particle mass-dimension ( $m$ - $D$ ) power law parameterizations to reduce the dimensionality of complex ice particle shapes. For a specific ice particle shape or an environmental condition, such relationship has the form:

$$m = \alpha D^\beta, \quad (1)$$

where both  $\alpha$  and  $\beta$  are constants over a specific size range. They are determined via direct measurements of ice particle mass and dimension (Locatelli and Hobbs, 1974; M90), or are constrained through aircraft measurements of the ice particle size distribution (PSD) and IWC (Heymsfield et al., 2010; Cotton et al., 2012). The prefactor  $\alpha$  was considered to contain information on particle density and thickness, whereas  $\beta$  was believed to have information on particle shape. We will discuss the latter in Sect. 4.1 for the riming process.”

The current ideas in this paper and comparison to observations are useful because they link theory with modeling and confirm the idea that light and moderate riming can be modeled with assuming fixed beta, and this method should improve models. But where does, for example, the fixed beta assumption break down? What are the limitations of the method?

Author response:

Your explanations are right and refer to phase 1 of riming growth in our paper. During phase 1, the shape of ice particles changes, but the maximum dimension  $D$  does not. That is, both the mass and projected area increase during phase 1 in a way that mass and area increase by rime-deposits filling in the gaps between branches in the case of dendrites, or making the column more spherical by expanding the  $a$ -axis. The assumption of conserved  $\beta$  and  $\delta$  appear valid in phase 1. The ice crystal growing by riming turns into a graupel particle at the end of phase 1. Once the graupel threshold is reached, phase 2 growth commences that describes the growth of quasi-spherical graupel. In this phase,  $D$  does increase due to riming, and so do mass and projected area. In particular, phase 1 is demonstrated by Eqs. (6)-(11), whereas phase 2 is explained by Eqs. (12)-(14). To better clarify and distinguish between these two phases, we added some explanations to the manuscript that explicitly mention phase 1 and 2:

abstract:

“... It was observed that  $\beta$  in the  $m$ - $D$  power law  $m = \alpha D^\beta$  appears independent of riming during the phase 1 (before the formation of graupel), with  $\alpha$  accounting for the ice particle mass increase due to riming. ... Once the graupel with quasi-spherical shape forms,  $D$  increases with an increase in  $m$  and  $A$  (phase 2 of riming). ...”

Page 16, starting from line 10:

“So far, we discussed the phase 1 of riming growth (before the formation of graupel), where  $m$  and  $A$  increases while  $D$  and therefore  $\beta$  and  $\delta$  are conserved. Once the graupel stage is attained, phase 2 of riming starts and the graupel continues to grow through riming, and a different methodology is required to describe riming growth at this growth stage, because graupel  $D$  increases by riming. ...”

Conclusions, first paragraph, page 25, starting from line 14:

“... To a good approximation under most conditions, riming does not increase (or decrease)  $\beta$  and  $D$  in an  $m$ - $D$  power law and the treatment of riming is simplified with riming increasing only  $\alpha$  during the phase 1 of riming (before the formation of graupel). ...”

Page 25, end of the first paragraph, starting from line 22:

“... Phase 2 of riming starts when graupel with quasi-spherical shape forms. In this phase, the increase in  $m$  and  $A$  causes an increase in  $D$ .”

General comments.

Why not show a plot of  $\alpha$  evolving or  $d\alpha/dt$ ?

Author response:  $d\alpha/dt$  is calculated in Eq. (24) and is implied from Fig. 6. Since  $D$  and  $\beta$  do not change by riming,  $d\alpha/dt$  is linearly proportional to  $dm/dt$ . We will show the change in  $\alpha$  with more details in our future paper (Erfani et al., 2017).

We added this sentence to Sect. 6, page 24, starting at line 4:

“... Since  $D$  and  $\beta$  do not change by riming,  $d\alpha/dt$  is linearly proportional to  $dm/dt$ .”

Page 3 Line 4 “mass of snow collected”

Author response: Corrected.

Lines 7-8 perhaps change “snowfall rate” to “precipitation rate”

Author response: We feel it is better not to change this since “snowfall rate” is used earlier in this paragraph, and the meaning is clear.

Line 10 40% (extra space)

Author response: Corrected.

Line 13 (QPEs)

Author response: Corrected

Line 14 remove (SGM) as it is only used one other time and not often

Author response: Done

Line 18 change to “mass sink”

Author response: We added the mass sink in this part:

“... should be affected by the mass sink, represented by the ice mass flux ...”

Line 21 change word “powerful”

Author response: We changed it to considerable

General comment: watch the spacing between number and deg C or other units

Author response: We checked all the units to make sure that there is a space between the number and unit, based on the ACP writing style.

Line 29 what is considered the western Arctic?

Author response: It refers to the Northwest Territories, Canada. This synonym is added to the sentence:

“... they happen nearly half of the time in the western Arctic, also known as Northwestern Territories, Canada (Shupe et al., 2006) ...”

Page 4 Lines 1-2 are confusing, reword

Author response: Changed to:

“... Moreover, such clouds are an important part of tropical convective storms, as airborne observations indicate large amounts of supercooled water in these storms (Rosenfeld and Woodley, 2000). ...”

Line 3 remove “tracks”, make storms on the previous line plural

Author response: Changed.

Line 6 this doesn't limit understanding of riming, instead it limits understanding of phase partitioning

Author response: Changed.

Line 9 riming peaks at -10.5C for low LWCs. Also, the reason is partly due to different collection efficiencies for planar versus isometric ice

Author response: We added this explanation to this sentence:

“They also showed that riming has a peak at -10.5 °C for low LWCs, where ice particles are isometric, and therefore have higher  $V$ . In addition, the reason is partly due to different collision efficiencies for planar versus isometric ice particles.”

Line 13 remove “process”

Author response: Changed

Line 14 “with a spherical shape”

Author response: Changed.

Lines 14-16 both sentences start with “In this”. Change

Author response: For the second one, “In this way” is changed to “Therefore”.

Line 23 give a better definition of alpha and beta

Author response: Since Equation (1) makes it obvious that  $\alpha$  is the prefactor and  $\beta$  is the power exponent, now we simply state: “where both  $\alpha$  and  $\beta$  are constants over a specific size range.”

It is not straightforward to define  $\alpha$  and  $\beta$  from a physical point of view, and this text is part of the Introduction. Most papers just say alpha and beta are constants. Nonetheless, we added this explanation to clarify these constants (page 5, starting at line 11):

“ $\alpha$  was considered to contain information on particle density and thickness, whereas  $\beta$  was believed to have information on particle shape. We will discuss the latter in Sect. 4.1 for the riming process.”

Page 5 Line 6 make clear that these are all different for different ice types

Author response: We clarified that this happens for a single crystal habit:

“For a specific ice habit, the  $m$ - $D$  and  $A$ - $D$  power laws are dependent on the size range considered, and it often takes two or even three  $m$ - $D$  power laws to describe a given  $m$ - $D$  relationship over all relevant sizes for that habit.”

Line 20 autoconversion isn't an actual word, so maybe just use conversion

Author response: “autoconversion” is now very common in the field of cloud microphysics modeling to describe the change from one ice category to another one in a model. Conversion is a general word that does not convey our purpose.

Line 20 “hydrometeor category to another”

Author response: Changed.

Line 24 “abrupt microphysical changes” to what?

Author response: To address this comment, we changed this sentence:

“...This is because the distinct boundaries between various ice hydrometeor categories impose abrupt changes in microphysical properties (such as ice particle mass, projected area, fallspeed, and effective diameter) from one hydrometeor category to another, while in nature the transition processes are gradual. ...”

Line 28 This isn't necessarily 4-moment because rime fraction and rime volume are not moments of the size distribution. You may want to ask Dr. Morrison about this.

Author response: We deleted “4-moment” from this sentence:

“... and was later used in a bulk model that prognoses number concentration, rime volume, rime mass and total mass. ...”

Line 29 there is no need to note about aggregation as it is not discussed in this paper

Author response: We deleted the mention of aggregation.

Page 6 Lines 1-2 you may want to better describe the method of MG09

Author response: We added new explanations to describe the method of MG08, in page 6, starting from line 1:

“...In this approach, different  $m$ - $D$  and  $A$ - $D$  expressions from the literature are used for either pure ice crystals or graupel. Then,  $m$  and  $A$  are calculated in a transitional step as a function of  $D$  and rimed mass fraction. Such  $m$ - $D$  and  $A$ - $D$  expressions resulted in a gradual transition from crystal mass to graupel mass. However, discontinuities were observed in transition between various  $A$ - $D$  expressions over the PSD because the size range for each microphysical step (ice crystal, graupel, and transition) was calculated in a way to provide only continuous mass, and thus produced discontinuities in projected area. ...”

Line 23 put  $Re$  in parentheses

Author response: Changed.

Line 24 what is a free fallspeed

Author response: We changed this sentence and mention that ice crystals were freely falling, compared to other studies in which ice crystals were suspended in the wind tunnel.

“Murakami et al. (1985) studied the  $E_c$  between polystyrene latex spheres ( $d < 6 \mu\text{m}$ ) and freely-falling planar ice crystals ( $1.5 \text{ mm} < D < 5 \text{ mm}$ , and  $70 < Re < 300$ ).”

Line 25 “that were exposed to”

Author response: Corrected.

Line 26 “Although  $d$  ranged”

Author response: Corrected.

Page 8 Line 21 “from the Sierra”

Author response: Corrected.

Line 29 and following line both start with Also

Author response: The former changed to “In addition”.

Page 9 Line 15 remove hyphens after moderately and heavily

Author response: Changed.

Line 17 add a year to the Magono and Lee citation

Author response: The year (1966) is added,

Page 10 Line 3 the binning intervals description is confusing.

Author response: To avoid the confusion, we added a table (Table 1) to better describe the bin intervals:

“Table 1. Description of the bin intervals of PSD.

bin number	bin lower point	bin upper point	bin width
1	100	200	100
2	200	300	100
3	300	400	100
4	400	500	100
5	500	600	100
6	600	700	100
7	700	800	100
8	800	900	100
9	900	1000	100
10	1000	1200	200
11	1200	1400	200
12	1400	1800	400
13	1800	2400	600
14	2400	3000	600
15	3000	4000	1000

”

Line 7 Do the results change if lightly rimed ice is assumed to be in the rimed ice category?

Author response: Since lightly rimed particles have characteristics more similar to unrimed particles, including them in rimed category would distort the rimed category in a way that the difference between rimed and unrimed mass would be less distinct. Moreover, there are very, very few ice particles in the SCPP dataset ( $\ll 1\%$ ) classified as “R1-” type crystals (denoting light riming). Since it was hard to distinguish between R1- and unrimed crystals during SCPP due to the magnification used, R1- was seldom used.

Figure 1 what density is assumed for the solid ice spheres?

Author response: Their density is equal to solid ice density ( $=0.917 \text{ g / m}^3$ ). We added this to this part of the manuscript:

“... The grey line, corresponding to spherical particles having density equal to  $0.917 \text{ g m}^{-3}$  (solid ice density), serves as an upper limit to ice particle mass. ...”

Lines 14-15 This is shown in Figure 2 and this should be noted

Author response: Although we explained this with more details for dendrites in Fig. 2, we also mentioned this for Fig. 1 to show the similar pattern for all SCPP ice particles. We added a sentence after these lines:

“... We discuss this with more details in Sect. 4.1. ...”

Page 11 Line 8 20-30% is less than others get and is less than the value of about a doubling of mass you use later in the paper. How can you explain this?

Author response: This ratio was for a subset of SCPP data that was used to produce Baker and Lawson (2006) m-A power law expression. To avoid confusion, we deleted this sentence. Note that it is consistent with M90 (who estimated 30-40%).

Line 15 perhaps start off by talking about methods that assume constant beta (MG09) and then corroborate their results

Author response: We discuss about this from Page 12 Line 17 to Page 13 Line 4.

Page 12 Eq 3 Can you also plot best fit values assuming  $D^3$ ? What reduced density values would you get if you assumed  $D^3$  and is this reasonable?

Author response: Assuming that unrimed dendrite mass conforms to the formula  $m = \rho_i \pi D^3 / 6$ , where  $\rho_i$  is ice density, such  $\rho_i$  is equal to  $0.07 \text{ g cm}^{-3}$  for  $D = 500 \text{ }\mu\text{m}$ . Note that this assumption would lead to a fit parallel to the ice spheres fit in Fig. 2, with a relatively low coefficient of determination ( $R^2 = 0.68$ ), compared to power law fit with  $R^2 = 0.97$ .

If we added this fit to Fig. 2, it would overlap with other fits in this figure (we already added unrimed and rimed dendrites and graupel m-D power law fits to this figure). Therefore, we added the above explanations to the manuscript, page 12, starting at line 14:

“... Assuming that unrimed dendrites mass conforms to the formula  $m = \rho_i \pi D^3 / 6$ , where  $\rho_i$  is a reduced density, such  $\rho_i$  is equal to  $0.07 \text{ g cm}^{-3}$  for  $D = 500 \text{ }\mu\text{m}$ . Note that this assumption would lead to a fit parallel to the ice spheres fit in Fig. 2, with relatively low coefficient of determination ( $R^2 = 0.68$ ), compared to power law fit with  $R^2 = 0.97$ . ...”

Lines 9-10 Put these statements in better context. Perhaps talk about how bulk models use graupel categories ( $D^3$ ) and some assume spherical snow, but others assume snow goes as  $D^2$ . Then talk about how beta should change in nature and the best way to parameterizing riming snow in models.

Author response: We changed the sentences after Eq. (5) to address this:

“...having an exponent nearly identical to that in Eq. (4) for heavily rimed dendrites. This is contrary to most cloud models that assume different ice categories (snowfall with  $\beta \sim 2$  and graupel with  $\beta \sim 3$ ) and an abrupt increase in  $\beta$  upon a change in ice category (autoconversion). Based on SCPP observations, it is apparent that the traditional hypothesis that  $\beta$  increases with riming is not correct, at least not before the graupel onset. ...”

Line 16 Again, if you assumed spherical graupel, what density would it have and could you also plot that m-D curve?

Author response: By assuming that initial graupel mass can be calculated as  $m = \rho_i \pi D^3 / 6$  where  $\rho_i$  is a reduced density, such  $\rho_i$  is equal to  $0.18 \text{ g cm}^{-3}$  for  $D = 500 \text{ }\mu\text{m}$ , which is lower than the  $\rho_i$  for heavily rimed graupel in the dry growth regime ( $\rho_i = 0.4 \text{ g cm}^{-3}$ ; Rutledge and Hobbs, 1984; Ferrier, 1994). However, this assumption would produce a fit parallel to the ice spheres fit in Fig. 2, and is poorly fitted to the SCPP R4b and R4c data ( $R^2 = 0.67$ ), compared to power law fit ( $R^2 = 0.94$ ).

If we added this fit to Fig. 2, it would have overlap with other fits in this figure (we already added unrimed and rimed dendrites and graupel m-D power law fits to this figure). Therefore, we added the above explanations to the manuscript, page 12, starting at line 17:

“By assuming that initial graupel mass can be calculated as  $m = \rho_i \pi D^3 / 6$  where  $\rho_i$  is a reduced density, such  $\rho_i$  is equal to  $0.18 \text{ g cm}^{-3}$  for  $D = 500 \text{ }\mu\text{m}$ , which is lower than the  $\rho_i$  for heavily rimed graupel in the dry growth regime ( $\rho_i = 0.4 \text{ g cm}^{-3}$ ; Rutledge and Hobbs, 1984; Ferrier, 1994). This assumption would produce a fit parallel to the ice spheres fit in Fig. 2, and is poorly fitted to the SCPP R4b and R4c data ( $R^2 = 0.67$ ), compared to the power law fit ( $R^2 = 0.94$ ).”

Page 13 Line 5 “beta as constant during the riming process (until spherical) for both”

Author response: Changed.

Line 8 perhaps use “number distribution” instead of “number density”

Author response: Changed.

Line 9 remove “because it is a function only of D”

Author response: Changed.

Lines 12-18 seem out of place

Author response: We moved this paragraph to Introduction (after the second paragraph in Sect. 1.1).

Line 20 this value is inconsistent with the 20-30% from earlier. Explain.

Author response: As explained previously, the value in this part is correct. The 20-30% value was based on a subset of SCPP that is now removed.

Page 14 Lines 1-3 you can probably just say this is due to errors in classification

Author response: This could be a classification error. However, we often see very large changes in  $m_r/m_u$  when only a few ice particles are sampled over a given size-interval. From our experience with this dataset, we feel that large variance in single ice particle mass within a given ice particle type category and size interval is not unusual. Therefore, the sentence was not changed, and it demonstrates the variance that poor statistics can generate.

Page 15 Line 10 Is this also justified because beta is approximately 2?

Author response: We changed the sentence to reflect this point:

“...This assumption can be justified, because  $m \propto \frac{\alpha}{\gamma} A$  (note that  $\beta$ ,  $\delta$  and  $D$  does not change during the phase 1 of riming); this can be investigated through future research..”

Line 19 The value of 3.3 will depend on things like rime density. Under what conditions does using this value work?

Author response: This should be generally valid for planar ice crystals. While “rime density” may vary considerably on a single particle basis, these results are for a population of graupel particles where these single-particle differences are averaged to provide a bulk value for the population.

Page 17 Line 5 again the value of 2.4 will depend on a lot of variable. When do you expect the model to break down?

This should be valid for the SCPP dataset. It is possible that graupel formed in Sierra Nevada snowstorms experiences more “wet growth” (i.e. cloud droplets do not immediately freeze upon impacting the ice crystal) whereas in Rocky Mountain snowstorms, graupel experiences primarily dry growth (droplets freeze immediately upon impact, resulting in lower “densities”), but this is speculation that cannot be tested within this SCPP dataset. Moreover, we do not know how much this might affect our results; we feel it is best not to speculate on this.

Page 22 Line 5 doesn't increasing size also lead to increasing Re?

Author response: In theory, Re also depends on D. However, when an ice particle falls in a mixed-phase cloud, riming causes an increase in its fallspeed, but not its maximum dimension.

Line 11 “as a conservative underestimate”

Author response: Changed.

Line 19 perhaps “number distribution”

Author response: Changed.

Line 21 it is assumed to be negligible, not zero

Author response: We changed this sentence:

“... Note that the cloud droplet sedimentation velocity  $v(d)$  is negligible compared to the ice particle fallspeed  $V(D)$  and was neglected in the similar equation by Heymsfield (1982), M95, and Zhang et al. (2014). ...”

Page 23 Line 7 “microphysical and therefore optical”

Author response: Many models use separate microphysical and optical parameterizations, and the variable in one parameterization might not depend on the other parameterization.

Page 24 Line 11 is it really  $d^{13}$ ?

Author response: Yes, because  $\nu = 9$ , and from Eq. (25) the dimension of  $n(D)$  is  $d^9 / d^{13} = d^{-4}$ .

Page 25 Line 11 should this be “representing ice particle m and D”?

Author response: Our methods calculated both projected area and mass. We used “mass” and “projected area” instead of “m” and “A” to avoid confusion.

Page 26 Line 1 change SGM to simple growth model

Author response: SGM stands for snow growth model. SGM has now been replaced by “snow growth model”.

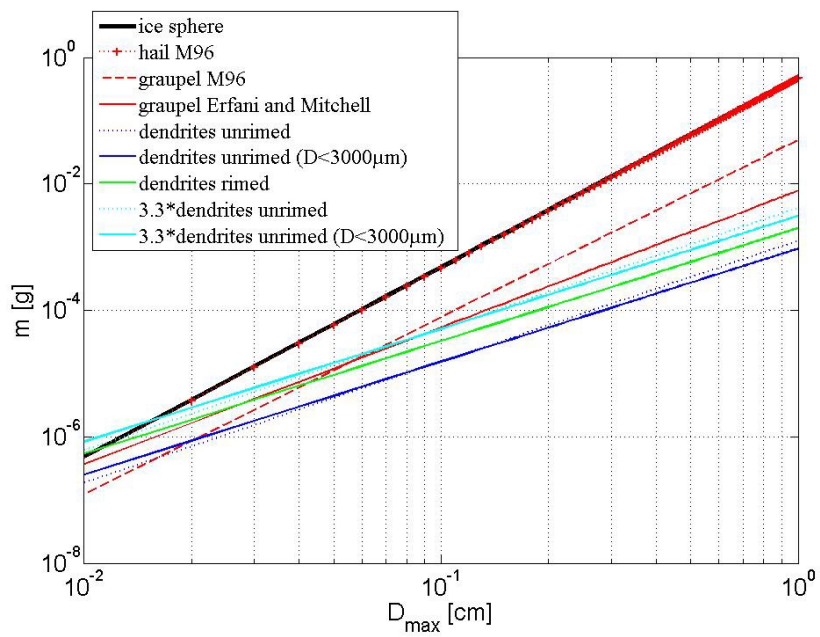


Fig. 1.

1

## 2 **Growth of ice particle mass and projected area during** 3 **riming**

4

5

6 **Ehsan Erfani<sup>1,2,\*</sup> and David L. Mitchell<sup>1</sup>**

7

8 [1] {Desert Research Institute, Reno, Nevada, USA}

9 [2] {Graduate Program in Atmospheric Sciences, University of Nevada, Reno, Nevada, USA}

10 [**\***] {Now at Center for Ocean-Land-Atmosphere studies, George Mason University, Fairfax,  
11 Virginia, USA}

12

13 Correspondence to: Ehsan Erfani (~~E~~Erfani@gmu.edu)

Deleted: [Ehsan@nevada.unr.edu](mailto:Ehsan@nevada.unr.edu)

14

15

16 Key points:

17 - Rimed particle projected area- and mass-dimension expressions are developed and validated.

18 - A convenient means of relating the unrimed and rimed  $m-D$  and  $A-D$  expressions was developed.

19 - Equations are provided to calculate collision efficiency for use in models.

20

1 **Abstract**

2 There is a long-standing challenge in cloud and climate models to simulate the process of ice  
3 particle riming realistically, partly due to the unrealistic parameterization of the growth of ice  
4 particle mass ( $m$ ) and projected area ( $A$ ) during riming. This study addresses this problem, utilizing  
5 ground-based measurements of  $m$  and ice particle maximum dimension ( $D$ ) and also theory to  
6 formulate simple expressions describing the dependence of  $m$  and  $A$  on riming. It was observed  
7 that  $\beta$  in the  $m$ - $D$  power law  $m = \alpha D^\beta$  appears independent of riming during the phase 1 (before  
8 the formation of graupel), with  $\alpha$  accounting for the ice particle mass increase due to riming. This  
9 semi-empirical approach accounts for the degree of riming and renders a gradual and smooth ice  
10 particle growth process from unrimed ice particles to graupel, and thus avoids discontinuities in  $m$   
11 and  $A$  during accretional growth. Once the graupel with quasi-spherical shape forms,  $D$  increases  
12 with an increase in  $m$  and  $A$  (phase 2 of riming). The treatment for riming is explicit, and includes  
13 the parameterization of the ice crystal-cloud droplet collision efficiency ( $E_c$ ) for hexagonal  
14 columns and plates using hydrodynamic theory. In particular,  $E_c$  for cloud droplet diameters less  
15 than 10  $\mu\text{m}$  are estimated, and under some conditions observed in mixed phase clouds, these  
16 droplets can account for roughly half of the mass growth rate from riming. These physically-  
17 meaningful yet simple methods can be used in models to improve the riming process.

18

19

20 Keywords: ice cloud microphysics, riming, collision efficiency, climate models, cloud models,

21

22

Formatted: Font:Italic, Complex Script Font: Not Italic

Formatted: Font:Italic, Complex Script Font: Not Italic

Deleted: two

Formatted: Font:Italic, Complex Script Font: Not Italic

# 1 Introduction

2 Observational studies have determined that the riming process contributes substantially to snowfall  
3 rates. Along the coastal plains of northern Japan, riming was responsible for 50% to ~100% of the  
4 mass of snow collected at ground level, which included graupel particles (Harimaya and Sato,  
5 1989). When only snowflakes were considered (no graupel), riming contributed between 40% and  
6 63% of the snow mass. In the Colorado Rocky Mountains, Feng and Grant (1982) found that, for  
7 the same number flux, the snowfall rate for rimed plates and dendrites was about twice the  
8 snowfall rate for unrimed plates and dendrites (implying that about half of the snowfall rate was  
9 due to riming). In the Sierra Nevada mountains of California, Mitchell et al. (1990; hereafter M90)  
10 estimated that riming contributed 30% to 40% of the mass of fresh snow during two snowfall  
11 events. Thus, an improved treatment of the riming process in cloud resolving models could  
12 significantly improve predicted snowfall amounts. This could also translate to improved  
13 quantitative precipitation estimates (QPEs) from National Weather Service radar systems during  
14 winter. For example, a simple snow growth model can be coupled with National Weather Service  
15 (NWS) radar reflectivity as described in Mitchell et al. (2006) to improve QPE, and adding the  
16 riming process should further improve these QPEs during winter storms.

Deleted: in

Deleted:

Deleted: (SGM)

17 The life cycle of Arctic mixed phase clouds, which strongly affect the Arctic energy budget and  
18 climate, should be affected by the mass sink, represented by the ice mass flux ( $M_f$ , all symbols are  
19 defined in Appendix A) at cloud base (representing a moisture sink). Riming has a strong impact  
20 on ice particle fallspeeds (Mitchell, 1996; hereafter M96), and  $M_f$  can be estimated as  $M_f = IWC \times$   
21  $V_m$ , where  $V_m$  is the mass-weighted fallspeed at cloud base and IWC is the ice water content. Since  
22 riming strongly contributes to both IWC and  $V_m$ , it has a considerable impact on  $M_f$ .

Deleted: powerful

## 24 1.1 Characteristics of Riming

25 Riming (accretion of supercooled water droplets on ice particles) occurs in mixed-phase clouds  
26 where ice particles and water droplets coexist at temperatures ( $T$ ) between  $-37.5\text{ }^\circ\text{C}$  and  $0\text{ }^\circ\text{C}$  in  
27 convective clouds in the Tropics (Rosenfeld and Woodley, 2000; Mitchell and d'Entremont,  
28 2012), and at  $-40.5\text{ }^\circ\text{C} < T < 0\text{ }^\circ\text{C}$  in wave clouds over continental mountains (Heymsfield and  
29 Miloshevich, 1993). Mixed-phase clouds are persistent in both the Arctic and in tropical regions,  
30 as they happen nearly half of the time in the western Arctic, also known as Northwestern

1 Territories, Canada (Shupe et al., 2006). Moreover, such clouds are an important part of tropical  
2 convective storms, as airborne observations indicate large amounts of supercooled water in these  
3 storms (Rosenfeld and Woodley, 2000). They also constitute a large portion of the cloud fraction  
4 in mid-latitude storms track (e.g. Hobbs, 1978; Matejka et al., 1980). However, a lack of  
5 observations in mixed-phase clouds (resulting from the challenge of detecting layers of  
6 supercooled liquid water in the ice-dominated parts of clouds) impeded an accurate computation of  
7 the liquid water content (LWC) to IWC ratio, which therefore limits an understanding of phase  
8 partitioning (Kalesse et al., 2016). Wind tunnel experiments by Takahashi and Fukuta (1988) and  
9 Fukuta and Takahashi (1999) measured the riming enhancement as an increase in ice particle  
10 fallspeed ( $V$ ). They also showed that riming has a peak at  $-10.5$  °C for low LWCs, where ice  
11 particles are isometric, and therefore have higher  $V$ . In addition, the reason is partly due to  
12 different collision efficiencies for planar versus isometric ice particles.

13 The wind tunnel experiment of Pflaum *et al.* (1979) showed that a cone-like graupel forms, when  
14 riming occurs on the bottom side of a falling planar crystal. However, if the particle flips over  
15 during fallout, a lump graupel forms ultimately. Heymsfield (1982) developed a parcel model, and  
16 demonstrated that growth of ice crystals by riming occurs on their minor axis, and therefore they  
17 evolve to graupel with a spherical shape of the same dimension. In this model, accreted mass fills  
18 in the unoccupied volume of the ultimately spherical graupel via riming growth. Therefore, ice  
19 particle mass increases while ice particle maximum dimension is conserved. The increase in  
20 dimension due to riming initiates once the ice particle obtains a spherical shape. This method was  
21 employed by several models to represent riming (Morrison and Grabowski, 2008; hereafter MG08;  
22 Morrison and Grabowski, 2010; Jensen and Harrington, 2015; hereafter JH15; Morrison and  
23 Milbrandt, 2015).

24 Note that riming occurs only when ice particles have a  $D$  greater than the riming threshold size  
25 ( $D_{\text{thres}}$ : the smallest ice crystal  $D$  for which riming can occur). Early observations (Harimaya,  
26 1975) and numerical studies (Pitter and Pruppacher, 1974; Pitter, 1977) determined a  $D_{\text{thres}}$  being  
27 around  $300 \mu\text{m}$ . However, it was later shown by both observational (Bruntjes et al., 1987) and  
28 numerical (WJ00) studies that such  $D_{\text{thres}}$  is around  $35 \mu\text{m}$ ,  $110 \mu\text{m}$ , and  $200 \mu\text{m}$  for hexagonal  
29 columns, hexagonal plates, and broad-branched crystals, respectively (note that all these  
30 dimensions are along a-axis of crystals).

Deleted: and they

Deleted: contribute to

Deleted: having

Deleted: s

Deleted: riming

Deleted: process

Deleted: In this way

Moved (insertion) [1]

1 Many models calculated ice particle mass by assuming that ice particles are spherical (e.g.  
2  $m = \rho_i \pi D^3 / 6$ , where  $\rho_i$  is ice density; Rutledge and Hobbs, 1984; Ferrier, 1994; Morrison and  
3 Gettelman, 2008). However, this assumption is not realistic, and produces errors in the evolution  
4 of snow-size spectra (Mitchell, 1988). Based on observations, several studies developed ice  
5 particle mass-dimension ( $m$ - $D$ ) power law parameterizations to reduce the dimensionality of  
6 complex ice particle shapes. For a specific ice particle shape or an environmental condition, this  
7 relationship has the form:

$$m = \alpha D^\beta, \quad (1)$$

8 where both  $\alpha$  and  $\beta$  are constants over a specific size range. They are determined via direct  
9 measurements of ice particle mass and dimension (Locatelli and Hobbs, 1974; M90), or are  
10 constrained through aircraft measurements of the ice particle size distribution (PSD) and IWC  
11 (Heymsfield et al., 2010; Cotton et al., 2012). The prefactor  $\alpha$  was considered to contain  
12 information on particle density and thickness, whereas  $\beta$  was believed to have information on  
13 particle shape. We will discuss the latter in Sect. 4.1 for the riming process. Similar power laws  
14 have been developed for projected area-dimension ( $A$ - $D$ ) relationships:

$$A = \gamma D^\delta, \quad (2)$$

15 where  $\gamma$  and  $\delta$  are constants over a specific size range derived by direct measurements of ice  
16 particle projected area and dimension (M96). When comparing rimed particles with the same size,  
17 lump graupel has the largest mass and area relative to cone-like graupel or hexagonal graupel, and  
18 densely rimed dendrites have still lower values (Locatelli and Hobbs, 1974; M96). For a specific  
19 ice habit, the  $m$ - $D$  and  $A$ - $D$  power laws are dependent on the size range considered, and it often  
20 takes two or even three  $m$ - $D$  power laws to describe a given  $m$ - $D$  relationship over all relevant  
21 sizes for that habit. To address this issue, Erfani and Mitchell (2016; hereafter EM16) developed a  
22 single  $m$ - $D$  and  $A$ - $D$  second-order polynomial curve fit in log-log space for  $20 \mu\text{m} \leq D \leq 4000 \mu\text{m}$   
23 for each cloud type (synoptic or anvil) and temperature range. Such expressions can easily be  
24 reduced to power laws for use in models and remote sensing, and provide size-dependent power  
25 law coefficients ( $\alpha$ ,  $\beta$ ,  $\gamma$  and  $\delta$ ). For this reason, they are useful for characterizing a gradual change  
26 in power law coefficients with ice particle growth. For more details on  $m$ - $D$  and  $A$ - $D$  expressions,  
27 see EM16.

Formatted: Font:Italic, Complex Script Font: Italic  
Field Code Changed

Deleted: uncertainties in models

Deleted: Many

Deleted: have

Deleted: relationships f

Deleted: s

Deleted: s

Deleted: such

Deleted: which

Deleted: ve

Deleted: is prefactor,

Deleted: and

Deleted: is power exponent, and both

Formatted: Font color: Auto

Deleted: T

1

## 2 1.2 Treatment of Riming in Models

Formatted: Heading 2, Left, Line spacing: single, Tabs: 0.38", List tab

3 Since explicit modeling of the riming process is computationally expensive, graupel and hail  
 4 categories were not considered in some bulk microphysics parameterizations used in some global  
 5 climate models or GCMs (Morrison and Gettelman, 2008; Gettelman and Morrison, 2015). The  
 6 common ice microphysics approach in most cloud and climate models is the separation of ice into  
 7 various hydrometeor categories such as cloud ice, snowflakes, and graupel (Rutledge and Hobbs,  
 8 1984; Ferrier, 1994; Fowler et al., 1996; Reisin et al. 1996; Morrison and Gettelman, 2008;  
 9 Gettelman and Morrison, 2015). The transition between various hydrometeors occurs by  
 10 autoconversion from one hydrometeor category to another. However, such autoconversion is  
 11 arbitrary and poorly constrained, and as shown by Eidhammer et al. (2014), cloud radiative  
 12 properties were sensitive to the choice of autoconversion threshold size in the Community  
 13 Atmosphere Model version 5 (CAM5). This is because the distinct boundaries between various ice  
 14 hydrometeor categories impose abrupt changes in microphysical properties (such as ice particle  
 15 mass, projected area, fallspeed, and effective diameter) from one hydrometeor category to another,  
 16 while in nature the transition processes are gradual.

Deleted: changes

17 To overcome this problem, MG08 advanced a bulk model that employed vapor diffusion and the  
 18 riming processes, and used multiple  $m$ - $D$  and  $A$ - $D$  power laws (Eqs. 1 and 2) to characterize ice  
 19 particles associated with different parts of the PSD. This method was applied to a bin model  
 20 developed by Morrison and Grabowski (2010), and was later used in a bulk model that prognoses  
 21 number concentration, rime volume, rime mass and total mass (Morrison and Milbrandt, 2015). In  
 22 this approach, different  $m$ - $D$  and  $A$ - $D$  expressions from the literature are used for either pure ice  
 23 crystals or graupel. Then,  $m$  and  $A$  are calculated in a transitional step as a function of  $D$  and rimed  
 24 mass fraction. Such  $m$ - $D$  and  $A$ - $D$  expressions resulted in a gradual transition from crystal mass to  
 25 graupel mass. However, discontinuities were observed in transition between various  $A$ - $D$   
 26 expressions over the PSD, because the size range for each microphysical step (ice crystal, graupel,  
 27 and transition) was calculated in a way to provide only continuous mass, and thus produced  
 28 discontinuities in projected area. JH15 developed a detailed ice growth model that simulates ice  
 29 particle habit and mass via the processes of vapor deposition and riming. This model is also a  
 30 single-category scheme, but it does not employ  $m$ - $D$  and  $A$ - $D$  power laws; instead, it computes the

Deleted: four-moment

Deleted: also included the process of ice particle aggregation

Formatted: Font:Italic, Complex Script Font: Italic

Formatted: Font:Italic, Complex Script Font: Italic

Deleted: ,

Formatted: Font:Italic, Complex Script Font: Italic

Formatted: Font:Italic, Complex Script Font: Italic

Deleted: are calculated

Formatted: Font:Italic, Complex Script Font: Italic

Deleted: smooth

Deleted: (continuous  $m$ - $D$  expressions over the PSD)

Deleted: ,

Deleted: ,

1 growth of ice particles along the major and minor axes of oblate or prolate spheroids (representing  
2 hexagonal plates or columns). Therefore, the model is able to simulate simple ice particle shapes,  
3 and also captures the temperature-dependency of vapor deposition and the riming processes (since  
4 particle shape is a function of temperature and relative humidity; Magono and Lee 1966;  
5 Pruppacher and Klett 1997). The simulated ice particle shape, mass, and fallspeed are in good  
6 agreement with observational data from wind tunnel experiments on ice crystal growth.

7 The computation of rime mass (an increase in ice particle mass by riming) in models is performed  
8 by calculating the accretional mass growth rate (Heymsfield, 1982; Mitchell, 1995; JH15). When  
9 an ice particle falls in a cloud of supercooled cloud droplets, the increase in its mass due to  
10 accretion depends on ice particle features (e.g. fallspeed and projected area), droplet characteristics  
11 (e.g. mass and number concentration of droplets), and the collision efficiency ( $E_c$ ) between an ice  
12 particle and droplet. More details on mass growth rates are provided in Sect. 6, and  $E_c$  is described  
13 in the next section.

Deleted: c

### 14 1.3 Collision Efficiency

15 One important factor in the modeling of riming is the calculation of the  $E_c$  between ice particles  
16 and cloud droplets (Pruppacher and Klett, 1997).  $E_c$  was calculated as a function of ice particle  $D$   
17 and cloud droplet diameter ( $d$ ) via both experimental measurements (Sasyo and Tokue, 1973,  
18 hereafter ST73; Kajikawa, 1974, hereafter K74; Murakami et al., 1985) and theoretical/numerical  
19 calculations (Beard and Grover, 1974; Pitter and Pruppacher, 1974; Schlamp, 1975; Pitter, 1977;  
20 Wang and Ji, 2000, hereafter WJ00). The difference in  $E_c$  between various studies is due to the  
21 strong sensitivity of  $E_c$  to the ice particle shape as well as the assumptions and limitations in  
22 different studies. Experimental measurements of  $E_c$  have been conducted in vertical wind tunnels.  
23 Such studies are rare due to the difficulty and limitations of experiments, and were limited to only  
24 planar ice crystals or circular disks with  $D > 1$  mm (Reynolds number,  $(Re) > 40$ ). Murakami et al.  
25 (1985) studied the  $E_c$  between polystyrene latex spheres ( $d < 6$   $\mu\text{m}$ ) and freely-falling planar ice  
26 crystals ( $1.5$  mm  $< D < 5$  mm, and  $70 < Re < 300$ ). ST73 investigated fixed hexagonal plates ( $5$   
27 mm  $< D < 20$  mm) that were exposed to water droplets contained in airflow in a vertical wind  
28 tunnel. Although  $d$  ranged from  $19$   $\mu\text{m}$  to  $41$   $\mu\text{m}$ , more than 80% of droplets had  $d$  between  $20$   $\mu\text{m}$   
29 and  $25$   $\mu\text{m}$ . K74 measured  $E_c$  via collection of water droplets ( $2.5$   $\mu\text{m} < d < 17.5$   $\mu\text{m}$ ) by freely-  
30 falling particles (both natural snow crystals and ice crystal models made of non-water substance)

Deleted: -

Deleted: collision efficiency (

Deleted: )

Deleted: or

Deleted: at their free fallspeeds

Deleted: are

Deleted: s

1 of various shapes (e.g. circular disks, hexagonal plates and broad-branched plates) with  $Re < 100$   
2 in a wind tunnel.

3 Numerical studies calculate the flow field around particles by solving the Navier-Stokes equation  
4 via numerical methods. The challenges for numerical studies are the complex shapes of ice crystals  
5 as well as the effect of turbulence. Early studies assumed steady state flow with simplified shapes  
6 such as an oblate spheroid with  $2 \leq Re \leq 20$  as an approximation for planar crystals (Pitter and  
7 Pruppacher, 1974; Pitter, 1977), and an infinite cylinder with  $0.2 \leq Re \leq 20$  as an approximation  
8 for columnar crystals (Schlamp, 1975). The main difference in  $E_c$  between experimental and  
9 numerical studies is observed for small droplets ( $d < 10 \mu\text{m}$ ), where numerical  $E_c$  is zero in this  
10 range, but the experimental results indicate finite  $E_c$ . As explained by K74, this difference might  
11 be due to the assumption of a steady flow field around the ice particle in the early numerical  
12 studies. WJ00 developed a numerical model of 3-D non-steady flow around pristine crystals (such  
13 as hexagonal plates with  $1 \leq Re \leq 120$  and columnar crystals of finite length and with  $0.2 \leq Re \leq$   
14  $20$ ) and water droplets ( $d < 200 \mu\text{m}$ ). Contrary to early numerical studies and in agreement with  
15 experimental results, they showed that  $E_c$  for small droplets has finite values for hexagonal plates  
16 (hexagonal columns) with  $Re \geq 10$  ( $Re \geq 0.2$ ).

17 Due to its expensive computation,  $E_c$  is sometimes assumed to be constant in the models (e.g.,  $E_c =$   
18  $0.75$  in MG08;  $E_c = 1$  in Rutledge and Hobbs, 1984; Ferrier, 1994; Fowler et al., 1996; Morrison  
19 and Milbrandt, 2015). Hall (1980; hereafter H80) provided an equation for  $E_c$  representative of  
20 hexagonal plates by fitting ellipse curves to the data of Pitter and Pruppacher (1974) and Pitter  
21 (1977). Although this relationship is practical and was used by several models (Morrison and  
22 Grabowski, 2010; JH15; Kalesse et al, 2016), it has limitations due to the natural shortcomings of  
23 the original numerical studies (assumptions of steady flow, ice oblate spheroids with  $Re < 20$  as an  
24 approximation for hexagonal plates, water droplets with  $d < 20 \mu\text{m}$ , and zero  $E_c$  for  $d < 10 \mu\text{m}$ ).  
25 WJ00 improved the computation of  $E_c$  by solving these issues, but did not provide an equation for  
26 use in the models. JH15 modified the equation from Beard and Grover (1974) for spherical  
27 raindrops in steady flow, and calculated  $E_c$  between prolate spheroids (as an approximation for  
28 hexagonal columns) and small water droplets.  $E_c$  calculated in this way compares well with the  
29 numerical study of WJ00 for  $5 \mu\text{m} < d < 20 \mu\text{m}$ .

1 Another challenge exists in the calculation of  $E_c$  between graupel and cloud droplets. Most studies  
2 used  $E_c$  from Beard and Grover (1974), and therefore assumed that this  $E_c$  is equal to the collision  
3 efficiency between raindrops and water drops (Reisin et al. 1996; Pinski et al. 1998; Khain et al.  
4 1999; Morrison and Grabowski, 2010). The justification for this assumption was the similar shape  
5 between graupel and raindrops. However, such particles have different natural features (e.g.,  
6 density and surface roughness). To solve this issue, Rasmussen and Heymsfield (1985) suggested  
7 that  $E_c$  between graupel and cloud droplets can be calculated by modification of the results of  
8 Beard and Grover (1974) for  $E_c$  between raindrops and water droplets. Similar to Beard and  
9 Grover (1974), they employed the superposition method for collision between particles, but they  
10 assumed that the small cloud droplets do not change the graupel fallspeed, therefore they used  
11 Stokes number instead of mixed Froude number in the non-dimensionalized momentum equation  
12 (see Eqs. 1-6 in Rasmussen and Heymsfield, 1985). On the other hand, von Blohn et al. (2009)  
13 investigated experimental  $E_c$  between freely falling spherical ice particles (initially  $580 \mu\text{m} < D <$   
14  $760 \mu\text{m}$ ) and water droplets ( $20 \mu\text{m} < d < 40 \mu\text{m}$ ) in a vertical wind tunnel with laminar flow.  
15 They showed that collection kernels of ice particles are higher than that of raindrops, and therefore  
16 calculated a correction factor to account for the error in  $E_c$ , when assuming raindrops instead of  
17 graupel.

18 The objective of this study is to develop various empirical and theoretical approaches to represent  
19 the continuous and gradual growth of ice particle mass and projected area during riming in a  
20 realistic and yet simple way, suitable for models. Section 2 of this study explains the data and  
21 method. In Sect. 3, results from a ground-based field campaign are applied to investigate  $m$ - $D$   
22 relationships during riming. Section 4 introduces a method to parameterize riming. In Sect. 5, new  
23 practical equations are presented to calculate  $E_c$  for hexagonal plates and hexagonal columns.  
24 Calculations of the mass growth rate due to riming are given in Sect. 6, and conclusions are  
25 provided in Sect. 7.

26

## 27 **2 Data and methods**

28 Ground-based direct measurements of  $m$  and  $D$  from the Sierra Cooperative Pilot Project (SCPP;  
29 see M90) during winter storms in Sierra Nevada Mountains are utilized in this study. SCPP was a  
30 field campaign on cloud seeding from 1986 to 1988, and for one part of that project, natural ice

1 particles were collected during snow storms in a polystyrene petri dish and then the particles were  
 2 photographed using a microscope equipped with a camera. Then a heat-lamp was used to melt  
 3 these ice particles, and immediately after melting another photograph was taken of the hemispheric  
 4 water drops (contact angle on polystyrene = 87.4 degrees). The images were used later in the lab to  
 5 measure the maximum dimension ( $D$ ) of individual ice particles (defined as diameter of a  
 6 circumscribed circle around the particle). In addition, the diameter of the water hemispheres was  
 7 measured, and from this the volume and mass of individual ice particles were computed. Also  
 8 recorded were individual ice particle shapes, which were classified using the Magono and Lee  
 9 (1966) nomenclature scheme. The level of riming (i.e. light, moderate, heavy riming, or graupel)  
 10 was indicated based on this scheme, and the temperature range over which the observed ice  
 11 particle shape originated was recorded (e.g. for long columns,  $-8^{\circ}\text{C} < T < -6^{\circ}\text{C}$ ). These riming  
 12 levels are indicated (with rimed crystal illustrations) in the Magono and Lee (1966) ice particle  
 13 classification scheme with the prefix R1, R2, R3 and R4 (see Pruppacher and Klett, 1997, p. 46).  
 14 Photographic examples of these rimed particle types are shown in Fig. 2 of Locatelli and Hobbs  
 15 (1974). Software was developed to extract all combinations of particle shapes (for a detailed  
 16 explanation of sampling and measurements, see M90). SCPP is a unique dataset that measures  
 17 both ice particle size and mass and also determines the degree of riming. As explained in EM16,  
 18 the important problem with airborne measurements is that they are unable to measure single ice  
 19 particle mass. Nonetheless, we compare our results with m-D relationships from previous studies  
 20 (Heymsfield et al., 2010; Cotton et al., 2012; EM16) that are based on airborne measurements.  
 21 EM16 provided  $m$ - $D$  curve fits based on Cloud Particle Imager (CPI) measurements from the  
 22 Department of Energy (DOE)-Atmospheric Radiation Measurement (ARM) funded Small  
 23 Particles In Cirrus (SPartICus) field campaign for  $D < 100 \mu\text{m}$  and a subset of SCPP data for  $D >$   
 24  $100 \mu\text{m}$ . Since CPI does not measure ice particle mass, EM16 developed a method that calculates  
 25 mass from the measurements of ice particle projected area,  $D$ , and aspect ratio by assuming that  
 26 small ice particles can be approximated as hexagonal columns (for more details, see Appendix B in  
 27 EM16). The subset of SCPP used in EM16 includes only unrimed ice particles that have habits  
 28 identical to those in cirrus clouds (selected based only on ice particles that have habits formed in  
 29 the temperature range between  $-40^{\circ}\text{C}$  and  $-20^{\circ}\text{C}$ ). There are 827 ice particles that are categorized  
 30 in this subset. Hereafter, this subset of SCPP data is referred to as “cold habit SCPP”. The SCPP  
 31 data has a total of 4869 ice particles, consisting of 2341 unrimed or lightly-rimed particles (such as

Deleted: Also

Deleted: indicated

Deleted: (if recognizable),

Deleted: basic

Deleted: e.g.,

Deleted: in

Deleted: ,

Deleted: deduced using diagrams from

Deleted: and

Deleted: (

Deleted: .

Deleted:

Deleted: maximum dimension

Deleted: is

1 plates, dendrites, columns, needles, bullets, bullet rosettes, side planes, and aggregates and  
2 fragments of these shapes), 1440 moderately or heavily rimed particles (such as rimed plates,  
3 rimed dendrites, rimed columns, and graupel), and 1088 unclassified particles. There were 118  
4 unrimed dendrites, including ordinary, stellar and fern-like dendrites, classified using the Magono  
5 and Lee (1966) scheme as P1e, P1d and P1f, respectively, as well as fragments and aggregates of  
6 these shapes. 80% of unrimed dendrites were P1e. Columnar crystals consisted of 262 N1e (long  
7 solid columns) and 337 C2b (combination of long solid columns) crystals. Some ice crystals  
8 classified as unrimed may be lightly rimed due to limitations in the magnification used. Moreover,  
9 852 particles were classified as heavily rimed dendrites, consisting of graupel-like snow of  
10 hexagonal type (R3a), graupel-like snow of lump type (R3b), and graupel-like snow with  
11 nonrimed extensions (R3c), of which 99% were R3b. These correspond to heavily rimed dendrites  
12 having graupel-like centers but with rimed branches extending outwards revealing the dendritic  
13 origin. Also classified were total of 67 lump graupel (R4b), cone-like graupel (R4c), and  
14 hexagonal graupel (R4a); R4b and R4c are graupel with non- discernable original habit, whereas  
15 R4a forms just prior to R4b or R4c, with its hexagonal origin still recognizable.

16 In order to represent the natural variability of ice particle mass, all identifiable particles are  
17 initially shown with their actual mass and maximum dimension. Thereafter, to quantify the  
18 variability and to further investigate  $m$ - $D$  power laws and the rimed-to-unrimed mass ratio, the ice  
19 PSDs were divided into size bins with intervals of 100  $\mu\text{m}$  between 100 and 1000  $\mu\text{m}$ , and with  
20 subsequent intervals of 200, 200, 400, 600, 600 and 1000  $\mu\text{m}$  (up to 4000 $\mu\text{m}$ ) at larger sizes to  
21 supply sufficient sampling numbers in each size bin (for more details on bin intervals, see Table  
22 1). In order to investigate the riming effect, all identifiable particles were sorted into either one of  
23 three rimed categories or an unrimed category. Both unrimed and lightly-rimed ice particles are  
24 included in the unrimed category, whereas the three rimed categories consist of densely rimed,  
25 heavily rimed, and graupel particles.

### 27 3 Measurements of ice particle mass and dimension in frontal clouds

28 The purpose of this section is to demonstrate how the cold habit SCPP curve fit from EM16 (based  
29 on unrimed ice crystals) compares with all the SCPP data, since this shows how the EM16 curve  
30 fit appears representative for all ice particles sampled during SCPP and thus may be representative

Deleted: -  
Deleted: -

Deleted: (Pruppacher and Klett, 1997)

Deleted: a  
Deleted: divided  
Deleted: d  
Deleted: ies  
Deleted: :  
Deleted: or  
Deleted: were classified  
Deleted: moderately  
Deleted: -  
Deleted: or  
Deleted: -  
Deleted: particles  
Deleted: were considered in rimed category  
Deleted:  
Deleted: investigate  
Deleted: CPI and  
Deleted: could indicate  
Deleted: this curve fit is

1 [for Sierra Nevada snowfall](#). This comparison is shown in Fig. 1a for all ice particles that could be  
2 classified (3781 ice particles). The curve fit appears to bisect the data well. [Moreover, it is seen](#)  
3 [that rimed ice particles tend to have larger mass on average, compared to unrimed ice particle of](#)  
4 [the same size. We discuss this with more details in Sect. 4.1.](#) Also displayed are the  $m$ - $D$  power  
5 law expressions from Cotton et al. (2012) and Heymsfield et al. (2010) that were acquired from  
6 synoptic ice clouds for  $-60\text{ }^{\circ}\text{C} < T < -20\text{ }^{\circ}\text{C}$  and from both synoptic and anvil ice clouds for  $-60\text{ }^{\circ}\text{C}$   
7  $< T < 0\text{ }^{\circ}\text{C}$ , respectively. The grey line, corresponding to spherical particles [having density equal to](#)  
8 [0.917 g m<sup>-3</sup> \(solid ice density\)](#), serves as an upper limit to ice particle mass. The Cotton et al.  
9 (2012) expression is composed of two power laws [that differ from](#) the EM16 curve fit [by less than](#)  
10 [50% \(over its size domain\)](#). The Heymsfield et al. (2010) expression is based on a single power  
11 law and [it](#) also estimates the curve fit well, except for the size ranges  $D > 1000\text{ }\mu\text{m}$  and  $D < 100$   
12  $\mu\text{m}$ , where the differences in mass can [reach](#) about 100%.

13 Figure 1b displays the EM16 curve fit along with all SCPP data (including those that could not be  
14 classified), where the ice PSDs were divided into size bins, as explained in Sect. 2. In this way,  
15 mean  $D$  and  $m$  in each size bin, and also the standard deviation ( $\sigma$ ) in each size interval for  $D$  and  
16  $m$ , are shown. Figure 1b shows that the [EM16](#) curve fit is well within the  $\sigma$  of SCPP mass and is  
17 [close](#) to the mean  $m$  for all size bins. The same is valid for the Cotton et al. (2012)  $m$ - $D$  line [over](#)  
18 [its size domain](#). The Heymsfield et al. (2010) line is within the  $\sigma$  of SCPP for  $250\text{ }\mu\text{m} < D < 1400$   
19  $\mu\text{m}$ . In order to be even more quantitative, the percent difference between the [total](#) SCPP mean ice  
20 particle mass in each size-bin of Fig. 1b and the corresponding mass from the cold habit SCPP  
21 curve fit from EM16 are computed (figure not shown). For  $D > 200\text{ }\mu\text{m}$ , percent differences are no  
22 more than 22%, with the curve fit slightly overestimating masses for  $D$  greater than  $1000\text{ }\mu\text{m}$ . This  
23 agreement might result partially from the riming of the planar ice crystals and aggregates thereof  
24 (adding mass with little change in size) and partially from an abundance of unrimed and rimed  
25 high density compact ice particles. Indeed, 38% of the ice particles were moderate-to-heavily  
26 rimed. [To summarize, it appears that the EM16 synoptic ice cloud curve fit for  \$-40\text{ }^{\circ}\text{C} < T \leq -20\text{ }^{\circ}\text{C}\$](#)   
27 [provides a realistic bulk estimate for ice particle masses in Sierra Nevada winter snowstorms at](#)  
28 [ground level](#).

**Deleted:** found in

**Deleted:** frontal clouds

**Deleted:** I

**Deleted:** also

**Deleted:** and accompanies

**Deleted:** significantly well for  $D > 100\text{ }\mu\text{m}$ , with differences in mass that never exceed 50%.

**Deleted:** extend to

**Deleted:** mostly adjacent

**Deleted:** mass

**Deleted:** when the

**Deleted:** is extrapolated to  $D > 500\mu\text{m}$

**Deleted:** only

**Deleted:** Based on the planar ice particles in this dataset (excluding side planes), we found that riming contributed to roughly 20-30% of ice particle mass on average for  $D > 700\text{ }\mu\text{m}$ , when riming was moderate-to-heavy.

**Deleted:** frontal clouds

29

## 1 4 Parameterization of riming

### 2 4.1 Dependence of $\beta$ and $\alpha$ on riming

3 A long-standing problem in cloud modeling is the treatment of  $\alpha$ ,  $\beta$ ,  $\gamma$  and  $\delta$  as a function of ice  
4 particle riming. Since riming leads to graupel formation and graupel tends to be quasi-spherical, it  
5 is intuitive to assume that  $\beta$  and  $\delta$  will approach limiting values of 3 and 2, respectively  
6 (corresponding to ice spheres), as more and more supercooled liquid water is accreted by an ice  
7 particle to produce graupel. One common approach in many cloud models (that use an  $m$ - $D$   
8 relationship) is to assume that  $\beta$  is equal to  $\sim 2$  for unrimed crystals and is equal to  $\sim 3$  for graupel.  
9 This implies that riming enhances  $\beta$ . This assumption is tested in this section by using SCPP data  
10 with the objective of developing observational-based guidelines for modeling the process of  
11 riming. To test this assumption for  $\beta$ , the size-resolved masses of rimed and unrimed ice particles  
12 from the same basic shape category are needed. In this section, we used heavily rimed dendrites  
13 (R3a, R3b and R3c) and unrimed dendrites (P1e, P1d and P1f). In addition, this data was  
14 partitioned into the same size-intervals described earlier to calculate the mean  $m$  and  $D$  in each  
15 size-interval for unrimed and heavily rimed dendrite crystals, along with their  $\sigma$ . All these results  
16 are shown in Fig. 2. Size-intervals having less than 3 measurements are not represented. Most of  
17 the data for unrimed crystals is associated with  $D > 600\mu\text{m}$ . One can see quantitatively how the  
18 mean masses for rimed dendrites are substantially greater than those for unrimed dendrites on  
19 average for the same size-interval, in agreement with the hypothesis of Heymsfield (1982).

20 Using only the size-intervals containing at least 3 measurements, the  $m$ - $D$  power law for the  
21 unrimed dendrites is:

$$m = 0.001263 D^{1.912}, \quad (3)$$

22 and for heavily rimed dendrites is:

$$m = 0.001988 D^{1.784}, \quad (4)$$

23 where all variables have cgs units. If the size-interval corresponding to the largest unrimed  
24 dendrites is not used in the least-square fit calculation, the  $m$ - $D$  expression for unrimed dendrites  
25 becomes:

$$m = 0.0009393 D^{1.786}, \quad (5)$$

Formatted: Font:Italic, Complex Script Font: Italic

Formatted: Font:Italic, Complex Script Font: Italic

1 having an exponent nearly identical to that in Eq. (4) for heavily rimed dendrites. This is contrary  
 2 to most cloud models that assume different ice categories (snowfall with  $\beta \sim 2$  and graupel with  $\beta$   
 3  $\sim 3$ ) and an abrupt increase in  $\beta$  upon a change in ice category (autoconversion). Based on SCPP  
 4 observations, it is apparent that the traditional hypothesis that  $\beta$  increases with riming is not  
 5 correct, at least not before the graupel onset. This can be understood by noting that  $\beta$  does not  
 6 necessarily indicate the morphology of an ice particle within a given size-interval, but rather  
 7 indicates the mass rate-of-change with respect to size (since  $\beta$  is the slope of the  $m$ - $D$  line in log-  
 8 log space). This can also be seen qualitatively in Fig. 2, where the rimed and unrimed data points  
 9 represent the same slope for the  $m$ - $D$  line in log-log space. Assuming that unrimed dendrites mass  
 10 conforms to the formula  $m = \rho_i \pi D^3 / 6$ , where  $\rho_i$  is a reduced density, such  $\rho_i$  is equal to  $0.07 \text{ g}$   
 11  $\text{cm}^{-3}$  for  $D = 500 \text{ }\mu\text{m}$ . Note that this assumption would lead to a fit parallel to the ice spheres fit in  
 12 Fig. 2, with relatively low coefficient of determination ( $R^2 = 0.68$ ), compared to power law fit  
 13 with  $R^2 = 0.97$ . In addition, the  $m$ - $D$  power law for lump graupel and cone-like graupel has the  
 14 form of  $m = 0.0078 D^{2.162}$  that represents a slight increase in  $\beta$  for graupel which is significantly less  
 15 than spherical  $\beta$  (which is equal to 3). By assuming that initial graupel mass can be calculated as  
 16  $m = \rho_i \pi D^3 / 6$  where  $\rho_i$  is a reduced density, such  $\rho_i$  is equal to  $0.18 \text{ g cm}^{-3}$  for  $D = 500 \text{ }\mu\text{m}$ ,  
 17 which is lower than the  $\rho_i$  for heavily rimed graupel in the dry growth regime ( $\rho_i = 0.4 \text{ g cm}^{-3}$ ;  
 18 Rutledge and Hobbs, 1984; Ferrier, 1994). This assumption would produce a fit parallel to the ice  
 19 spheres fit in Fig. 2, and is poorly fitted to the SCPP R4b and R4c data ( $R^2 = 0.67$ ), compared to  
 20 the power law fit ( $R^2 = 0.94$ ).

21 All these observations are in agreement with the experiment of Rogers (1974) in which  $\beta$  was  
 22 similar for unrimed and rimed snowflakes. The results of Rogers (1974) were used in the modeling  
 23 work of MG08 and Morrison and Grabowski (2010) to assume that riming does not change  $\beta$  for  
 24 planar ice crystals. Morrison and Milbrandt (2015) used a similar assumption based on the  
 25 observations of Rogers (1974) and Mitchell and Erfani (2014), and they explained that the reason  
 26 for the conservation of  $\beta$  during riming is the fact that  $D$  does not significantly change by riming  
 27 while  $m$  does increase significantly. A similar assumption is also valid for hexagonal columns. The  
 28 impact of moderate to heavy riming on  $\beta$  for hexagonal columns was demonstrated in M90 (see  
 29 their Table 1 and Sect. 4d). For these columnar crystals, riming had no effect on  $\beta$  (i.e.,  $\beta$  was 1.8  
 30 for both rimed and unrimed columns), indicating that riming can be modeled by only increasing  $\alpha$

Deleted: I  
 Deleted: now  
 Deleted: not for these measurements

Field Code Changed

Field Code Changed

Deleted: However, t

Deleted: ice particle maximum dimension

1 for these crystals. Thus, it appears justified to treat  $\beta$  as constant during the riming process (until  
 2 spherical shape) for both dendritic and columnar ice crystals:

$$\beta = \beta_u, \quad (6)$$

3 where subscript  $u$  denotes unrimed conditions. The IWC is defined as:

$$\text{IWC} = \int m(D)n(D)dD = \alpha \int D^\beta n(D)dD \quad (7)$$

4 where  $n(D)$  is number distribution. We explained that  $\beta$  and  $D$  do not change during riming. Also  
 5 unchanged is  $n(D)$ , because the number of ice particles in each size bin is not affected by riming.  
 6 Therefore, the dependence of  $\alpha$  on riming can be calculated by knowing the contribution of riming  
 7 to the IWC:

$$\frac{\alpha}{\alpha_u} \approx \frac{\text{IWC}}{\text{IWC}_u}. \quad (8)$$

8  
 9 Since  $\beta$  is essentially the same in Eqs. (4) and (5), their prefactor ratio ( $\alpha$  in Eq. 4 divided by  $\alpha$  in  
 10 Eq. 5, which is equal to 2.12) indicates that riming contributed slightly more than half the mass of  
 11 the rimed dendrites. This can be confirmed by calculation of ratio of mean rimed dendrite mass  
 12 ( $m_r$ ) to mean unrimed dendrite mass ( $m_u$ ) for each common size-interval, as shown in Fig. 3. This  
 13 riming ratio ( $m_r/m_u$ ) for each size-bin varies from  $\sim 0.5$  to 3 with many values close to 2. The  
 14 weighted average of  $m_r/m_u$  is equal to 2.0, supporting the first estimate of 2.12. The largest  
 15 deviation from the mean for  $300 \mu\text{m} < D < 400 \mu\text{m}$  may be due to only a single unrimed ice crystal  
 16 of anomalous mass in this size bin.

17 Equations (4) and (5) also suggest a means of adapting the  $m$ - $D$  curve fit in Fig. 1 for modeling the  
 18 riming process in mixed phase clouds. Since this curve fit is representative of ice particle  
 19 populations in frontal clouds (containing a mixture of unrimed and rimed particles), it can be  
 20 adapted for modeling the riming process in frontal clouds. Since  $\beta$  should be essentially the same  
 21 for both unrimed and the mixture of unrimed plus rimed SCPP ice particles, the ratio of their  
 22 corresponding prefactors (i.e.  $\alpha_u/\alpha_{mix}$ ) can be multiplied by the mass predicted by the curve fit  
 23 equation to yield the masses appropriate for unrimed particles. For the ice particles plotted in Fig.  
 24 1a,  $m_u/m_{mix}$  is equal to 0.650 (where  $m_{mix}$  includes all these particles and  $m_u/m_{mix}$  was calculated by

Deleted: density

Deleted: it is a function only of  $D$ , and

Moved up [1]: Note that riming occurs only when ice particles have a  $D$  greater than the riming threshold size ( $D_{\text{rim}}$ : the smallest ice crystal  $D$  for which riming can occur). Early observations (Harimaya, 1975) and numerical studies (Pitter and Pruppacher, 1974; Pitter, 1977) determined a  $D_{\text{rim}}$  being around  $300 \mu\text{m}$ . However, it was later shown by both observational (Brunjes et al., 1987) and numerical (W100) studies that such  $D_{\text{rim}}$  is around  $35 \mu\text{m}$ ,  $110 \mu\text{m}$ , and  $200 \mu\text{m}$  for hexagonal columns, hexagonal plates, and broad-branched crystals, respectively (note that all these dimensions are along a-axis of crystals).

1 the same method that calculated  $m_r/m_u$  in Fig. 3). This implies that multiplying the mass predicted  
2 by the curve fit in Fig. 1 by a factor of 0.65 will yield masses proper for unrimed ice particles. To  
3 model the riming process in frontal clouds, these unrimed particles can be subjected to the riming  
4 growth equations described below as well as Eq. (8).

5

## 6 **4.2 Dependence of $\delta$ and $\gamma$ on riming**

7 MG08 used different  $A$ - $D$  power laws in each riming step, but such method led to discontinuities  
8 in projected area during the transition from one ice category to another one. It seems that the  $A$ - $D$   
9 and  $m$ - $D$  that they used were not self-consistent (e.g. they were from on different studies based on  
10 different datasets). Here, we suggest an approach to avoid the discontinuity in projected area.

Formatted: Font:Italic, Complex Script Font: Italic

Formatted: Font:Italic, Complex Script Font: Italic

Formatted: Font:Italic, Complex Script Font: Italic

11 Since there are no SCPP  $A$ - $D$  measurements that correspond with the  $m$ - $D$  measurements used in  
12 Sect. 4.1, a purely empirical evaluation of the dependence of  $\delta$  and  $\gamma$  on riming was not possible.  
13 However, Fontaine et al. (2014) simulated numerous ice particles (pristine crystals, aggregates,  
14 and rimed particles) with various 3-D shapes and also their projected area (assuming random  
15 orientation). By this, they were able to develop a linear expression between  $\beta$  and  $\delta$ . This linear  
16 expression implies that  $\delta$  is constant during the riming process, since  $\beta$  has no riming dependency  
17 (see Sect. 4.1):

$$\delta = \delta_u \quad (9)$$

18 The reason for this can be explained by noting that the riming process often affects  $A$  but does not  
19 change  $D$  (by filling the space between ice particle branches) significantly prior to graupel  
20 formation. This is also evident from observations, as shown in Table 1 of M96, where  $\delta$  is equal to  
21 2 for both hexagonal plates and lump graupel. For constant  $\delta$ , only  $\gamma$  depends on riming, and to  
22 express  $\gamma$  as a function of riming, we developed a method that estimates the change in  $A$  by riming  
23 as a function of the change in  $m$ :

$$A = (A_{\max} - A_u)R + A_u \quad (10)$$

24 where  $A_{\max}$  is the maximum projected area due to riming in the phase 1 (which is the graupel  $A$ ),  
25 and  $R$  is the riming factor defined as:

$$R = \frac{m - m_u}{m_{\max} - m_u} \quad (11)$$

1 where  $m_{\max}$  is the graupel  $m$  (having the same  $D$  as  $m$  and  $m_u$ ).  $R$  is between 0 and 1, with 0  
 2 denoting no riming and 1 indicating graupel formation. In other words, when an ice crystal is  
 3 unrimed,  $m = m_u$  and  $A = A_u$ ; and when  $m = m_{\max}$  and  $A = A_{\max}$ , the ice crystal attains graupel  
 4 status at the end of phase 1. For a given  $D$ ,  $\gamma = A / D^\delta$ , and in this way the riming dependence of  $\alpha$   
 5 and  $\gamma$  can be treated, while  $\beta$  and  $\delta$  are independent of riming. Note that Eq. (10) assumes a linear  
 6 relationship between  $m$  and  $A$  during riming. This assumption can be justified, because  $m \propto \frac{\alpha}{\gamma} A$   
 7 (note that  $\beta$ ,  $\delta$  and  $D$  does not change during the phase 1 of riming); this can be investigated  
 8 through future research.

Deleted: ,  
 Field Code Changed

Deleted: , but  
 Deleted: an assumption that  
 Deleted: it  
 Formatted: Font:Italic, Complex Script Font: Italic

#### 10 4.2.1 Planar ice crystals

11 Using the approach above,  $m$  (in particular,  $\alpha$ ) should first be determined as a function of riming  
 12 using conventional theory (this will be discussed in Sect. 6), and then Eqs. (8), (10) and (11) can  
 13 be applied to calculate  $A$ . In order to determine  $m_{\max}$ , we calculated the  $m_r/m_u$  that corresponds to  
 14 graupel (R4a, R4b, and R4c) and unrimed dendrites (P1d, P1e, and P1f), as shown in Fig. 4a.  
 15 Small variability is seen for  $D < 1200 \mu\text{m}$  (ranges from 3 to 3.8, with the exception of smallest size  
 16 bin), whereas large variability exists (between 1.6 and 8.4) for larger sizes due to the small number  
 17 of graupel in each size bin. The weighted average for this  $m_r/m_u$  ratio is equal to 3.3 which can be  
 18 used to estimate  $m_{\max}$ :  $m_{\max} \approx 3.3 \times m_u$  for the dendrites. Since R4a occurs just before hexagonal  
 19 features are completely obscured by additional rime deposits, R4a graupel is ideal for estimating  
 20  $m_{\max}$ . Unfortunately, there are only 14 R4a particles in the entire SCPP data, with  $D < 1200 \mu\text{m}$ .  
 21 They exhibit a large variability in the  $m_r/m_u$  ratio (ranging from 1.6 to 4.5) with a weighted  
 22 average of  $m_r/m_u$  equal to 3.1 (figure not shown). Nonetheless the close agreement with the above  
 23  $m_r/m_u$  ratio of 3.3 is encouraging for us to conclude that initial graupel mass (at the end of phase 1)  
 24 is 3.3 times larger than unrimed dendrites. Since the SCPP observations show that  $D$  and  $\beta$  are  
 25 conserved during the phase 1 of riming, graupel density is also  $\sim 3.3$  times larger than unrimed  
 26 dendrite mass. A similar observational analysis was conducted by Rogers (1974), who found that  $\alpha$

Formatted: Font:Italic, Complex Script Font: Italic  
 Formatted: Font:Italic, Complex Script Font: Italic

1 for heavily rimed snowflakes was 4 times larger than that for unrimed snowflakes (and  $\beta$  was  
2 similar for both rimed and unrimed snowflakes). Since there is no observation to indicate  $A_{\max}$ , it  
3 can be approximated as the area of a circle having the same  $D$  ( $A_{\text{sphere}}$ ); but since graupel is not  
4 perfectly spherical,  $A_{\max}$  can be better estimated as a fraction of  $A_{\text{sphere}}$ ;  $A_{\max} = kA_{\text{sphere}}$ , where  $k$  is  
5 correction factor. Heymsfield (1978) analyzed graupel particles in northeastern Colorado, and  
6 found that their aspect ratio does not exceed 0.8. Using this value, JH15 showed good agreement  
7 between their model and observational data from a wind tunnel. Based on such analysis,  $k$  is equal  
8 to 0.8. Further observational data are needed to determine the value of  $A_{\max}$  more accurately.

9 *So far, we discussed the phase 1 of riming growth (before the formation of graupel), where  $m$  and*  
10  *$A$  increases while  $D$  and therefore  $\beta$  and  $\delta$  are conserved. Once the graupel stage is attained, phase*  
11 *2 of riming starts and* the graupel continues to grow through riming, and a different methodology  
12 is required to describe riming growth at this growth stage, because graupel  $D$  increases by riming.  
13 Once  $m = m_{\max}$ , then a graupel bulk density is defined as:

$$\rho_g = \frac{m_{\max}}{V_g} \quad (12)$$

14 Where  $V_g = (\pi/6)D_g^3$  and  $D_g$  is graupel  $D$  when  $m = m_{\max}$ . For subsequent riming growth,  $\rho_g$   
15 remains constant. For this growth stage, riming does increase  $D$  and  $A$ , which are determined as a  
16 function of riming as:

$$D = \left( \frac{6m}{\pi\rho_g} \right)^{\frac{1}{3}} \quad (13)$$

$$A = k \frac{\pi}{4} D^2 \quad (14)$$

17 where  $m$  is calculated as described in Sect. 6. As before, for a given  $D$ ,  $\gamma = A/D^3$ , and in this way  
18 riming growth is treated for all conditions.

19

Deleted: -

Formatted: Font:Italic, Complex Script Font: Italic

Formatted: Font:Italic, Complex Script Font: Italic

Formatted: Font:Italic, Complex Script Font: Italic

Formatted: Font:Italic, Font color: Auto, Complex Script  
Font: Italic

Formatted: Font color: Auto

Formatted: Font:Italic, Font color: Auto, Complex Script  
Font: Italic

1 **4.2.2 Columnar ice crystals**

2 Figure 4b represents  $m_r/m_u$  between graupel (R4b and R4c) and unrimed columnar crystals (N1e  
3 and N2c) in order to determine  $m_{max}$  for columnar crystals (initial graupel at the end of phase 1).  
4 Relatively small variability of  $m_r/m_u$  (between 1.6 and 3) is found for  $D < 1400 \mu m$ , with larger  
5 variability (from 1.4 to 9.4) found for larger ice particles, with the weighted average of  $m_r/m_u$   
6 equal to 2.4, and therefore  $m_{max} \approx 2.4 \times m_u$ . The higher variability for  $D > 1400 \mu m$  is likely due to a  
7 single graupel particle per size-bin. Based on SCPP dataset, we showed that  $D$  and  $\beta$  are constants  
8 during the phase 1 of riming, and since initial graupel mass is 2.4 times larger than unrimed  
9 column mass, these mean that graupel density is  $\sim 2.4$  times larger than unrimed column density.

Formatted: Font:Italic, Complex Script Font: Italic

Formatted: Font:Italic, Complex Script Font: Italic

11 **4.3 Testing the Baker and Lawson (2006)  $m-A$  expression with unrimed dendrites**

12 Some of the data shown in Fig. 2 describes an experiment investigating the ability of the Baker and  
13 Lawson (2006) (hereafter BL06)  $m-A$  power law to reproduce the masses of unrimed dendrites that  
14 presumably have relatively low area ratios (the ratio of the actual ice particle projected area to the  
15 area of a circle having a diameter equal to  $D$ ). A study by Avramov et al. (2011) found that this  
16 power law overestimated the masses of low-density dendrites (P1b), high-density dendrites (P1c),  
17 and low density dendrite aggregates, but that the BL06 power law yielded masses consistent with  
18 high density dendrite aggregates at commonly observed sizes. It is important to understand the  
19 potential limitations of this power law for dendrites due to their abundance in Arctic mixed phase  
20 clouds and for the modeling of these clouds. BL06 used a subset of SCPP data (e.g. 865 ice  
21 particles), of which 550 were identifiable, and 36% of such identifiable particles were moderately  
22 or heavily rimed. They then developed a software to calculate ice particle projected area from their  
23 magnified images. Thereafter, they calculated a  $m-A$  power law expression. Since BL06 used only  
24 a subset of the SCPP data to produce a  $m-A$  relationship (i.e. not a  $m-D$  relationship), comparison  
25 of their work and our study is meaningful. Unfortunately, there were only 7 unrimed and 2 lightly  
26 rimed dendrites in the BL06 dataset to investigate this finding. These are represented in Fig. 2 by  
27 green circles; their masses were calculated from the BL06  $m-A$  expression using their measured  
28 projected areas. For  $D < 1.4 mm$ , the BL06 unrimed dendrite masses are consistent with the  
29 unrimed dendrite masses from all SCPP data evaluated in this study (e.g., are within  $\pm 1 \sigma$  of mean  
30  $m$  for each size-bin), but at larger sizes the BL06 unrimed dendrite masses conform with rimed

Deleted: the ice particle maximum dimension

Formatted: Font color: Auto

Deleted: )

Deleted: and used a different curve fit (

Formatted: Font color: Auto

Formatted: Font color: Auto

Deleted: (and not all SCPP

Formatted: Font color: Auto

Deleted: and

Formatted: Font color: Auto

Formatted: Font color: Auto

Formatted: Font color: Auto

Deleted: )

Formatted: Font color: Auto

Deleted:

1 dendrite masses evaluated in this study. This suggests that for  $D > 1.4$  mm, the BL06  $m$ - $A$   
2 expression might overestimate the masses of unrimed dendrites by about a factor of two. This is  
3 broadly consistent with Avramov et al. (2011) for the size range considered. However, there is  
4 insufficient data here to draw any firm conclusions.

5 Although  $A$  is more strongly correlated with ice particle  $m$  than is  $D$  (based on BL06), inferring  $m$   
6 or volume from a 2-D measurement is still ambiguous since different crystal habits exhibit  
7 different degrees of ice thickness or volume for a given  $A$ . Thus, the BL06  $m$ - $A$  expression is not  
8 expected to be universally valid for all ice crystal habits. On the other hand, when applied to  $A$   
9 measurements in cirrus clouds, it yields ice particle mass estimates that are very consistent with  
10 two other studies that estimated  $m$ - $D$  expressions for cirrus clouds (Heymsfield et al., 2010; Cotton  
11 et al., 2012), as described in Sect. 3. In addition, a comparison with a cold-habit SCPP dataset  
12 provided additional evidence that the BL06  $m$ - $A$  expression yields masses appropriate for ice  
13 particles found in cirrus clouds. It also yields masses that are very consistent with the mean masses  
14 obtained for all ice particles sampled during the SCPP, indicating that the BL06  $m$ - $A$  expression  
15 appears representative of ice particle masses characteristic of Sierra Nevada snow storms. As  
16 explained by EM16 and references therein, there is only about a 20% difference between IWCs  
17 calculated from PSD using the BL06  $m$ - $A$  power law and collocated direct measurements of IWC  
18 in tropical regions; however, such differences can be as high as 100% in Polar Regions.

19

## 20 **5 Collision Efficiencies**

21 As mentioned in Sect. 1.2, there is a lack of practical methods in the literature for computing  $E_c$  for  
22 plates, columns, and graupel. In this section, equations are provided that calculate  $E_c$  for hexagonal  
23 plates and hexagonal columns, based on the data of WJ00. Such equations can be used in cloud  
24 and climate models to treat the riming process.

### 25 **5.1 Hexagonal plates**

26 The numerical study of WJ00 is valid for unsteady flow, hexagonal ice plates with  $1 < \text{Re} < 120$   
27 and  $160 \mu\text{m} < D < 1700 \mu\text{m}$ , and water droplets ~~having diameter  $d$  between,  $1 \mu\text{m}$  and,  $100 \mu\text{m}$ .~~  $\text{Re}$   
28 for hexagonal plates is calculated based on  $\underline{D}$  (e.g.,  $\text{Re}_{\text{plates}} = DV/\varepsilon$ , where  $\varepsilon$  is kinematic

Deleted: with

Deleted:  $< d <$

Deleted: the maximum dimension

1 viscosity). Since there is not sufficient agreement between the historical H80 relationship and the  
 2 data of WJ00, we provided best fits to the data of WJ00 that has the form of:

$$E_c = \begin{cases} (0.787K^{0.988})(0.263\ln Re - 0.264), & 0.01 \leq K \leq 0.35 \quad \& \quad 2 < Re \leq 120 \\ (0.7475 \log K + 0.620)(0.263\ln Re - 0.264), & 0.35 < K \leq K_{thres} \quad \& \quad 2 < Re \leq 120 \\ \sqrt{1 - \frac{1}{5} \left[ \log\left(\frac{K}{K_{crit}}\right) - \sqrt{5} \right]^2}, & K_{thres} < K < 35 \quad \& \quad 1 \leq Re \leq 120 \end{cases} \quad (15)$$

3 where  $K$  is mixed Froude number of the system of water drop-ice particle, and is calculated as:

$$K = \frac{2(V-v)v}{Dg}, \quad (16)$$

4 where  $v$  is water drop fallspeed, and  $g$  is gravitational acceleration. Since cloud water drops are in  
 5 Stokes regime,  $v$  is calculated as the Stokes fallspeed (e.g.,  $v = g(\rho_w - \rho_a)d^2 / 18\mu$ , where  $\rho_w$  is  
 6 water density,  $\rho_a$  is air density, and  $\mu$  is dynamic viscosity), and  $K$  is the same as the Stokes  
 7 number in this flow regime.  $K_{crit}$  is the critical value of  $K$  (where  $E_c$  equals 0 in the third line in Eq.  
 8 15) and is expressed as a function of ice particle  $Re$ :

$$K_{crit} = \begin{cases} 1.250 Re^{-0.350}, & 1 < Re \leq 10 \\ 1.072 Re^{-0.301}, & 10 < Re \leq 40 \\ 0.356 Re^{-0.003}, & 40 < Re \leq 120 \end{cases} \quad (17)$$

9 Based on Eq. (15),  $E_c$  in the third line is physically meaningful only when  $K \geq K_{crit}$ . When  $K <$   
 10  $K_{crit}$ ,  $E_c$  in the third is imaginary and must be set to zero in order to avoid errors.  $K_{thres}$  is the  
 11 threshold of  $K$  between small and large cloud droplets, and is calculated as:  
 12  $K_{thres} = -5.07 \times 10^{-10} Re^5 + 1.73 \times 10^{-7} Re^4 - 2.17 \times 10^{-5} Re^3 + 0.0013 Re^2 - 0.037 Re + 0.8355$ , and has  
 13 values between 0.4 and 0.7. Alternatively, it can be calculated for a desired  $Re$  by equating  $E_c$  from  
 14 the second line with  $E_c$  from the third line in Eq. (15) (e.g., finding the intersection of curves  
 15 defined by the second and the third lines of Eq. 15) to avoid any discontinuity. The third line in Eq.  
 16 (15) is an ellipse fit similar to H80 equation, but such a fit cannot represent finite values of  $E_c$  for  
 17 small drops (when  $K < K_{thres}$ ), and therefore this ellipse fit is not valid for small drops. To  
 18 overcome this issue, curve fits are developed (the first and second lines in Eq. 15) similar to

1 Mitchell (1995; hereafter M95). M95 provided curve fits to experimental  $E_c$  data described in  
2 ST73, K74 and Murakami et al. (1985) that showed slight sensitivity to  $Re$ . Here, those equations  
3 are modified and additional terms are employed to account for the  $Re$  dependence of  $E_c$  for small  
4 droplets, based on the data of WJ00.

5 The resulting curve fits for  $E_c$  (Fig. 5a) show that the provided equations can represent the data of  
6 WJ00 very well in various ranges of  $K$  and  $Re$ . The percent error in  $E_c$  between curve fits and  
7 WJ00 data has a mean value of 6.65% with standard deviation of 3.67% for all  $Re$  and  $K$ . For a  
8 given  $K$ ,  $E_c$  for planar crystals increases with an increase in  $Re$  because of the increase in the  
9 plate's fallspeed. In addition,  $E_c$  has a slight sensitivity to  $Re$  for  $Re \geq 60$ .  $E_c$  for small  $Re$  ( $Re \leq 2$ )  
10 appears to have a different pattern than that for larger  $Re$ , since  $E_c$  has zero values for small water  
11 drops ( $K \leq 1$ ). This implies that smaller ice particles that have sizes slightly larger than the  $D_{thres}$   
12 are incapable of collecting the smaller drops. For a given  $Re$ ,  $E_c$  increases with increasing  $K$ ,  
13 associated with an increase in droplet diameter, but it does not exceed a value of unity. For  
14 comparison, historical experiments by ST73 and K74 are also shown in this graph. K74 data for  $10$   
15  $\leq Re \leq 35$  is in good agreement with the curve fit for  $Re = 10$ . Values of  $E_c$  from K74 for  $200 \leq Re$   
16  $\leq 640$  are slightly lower than curve fit for  $Re = 120$ . This does not seem to be a discrepancy,  
17 because it is observed from the curve fits (based on WJ00) that  $E_c$  is not sensitive to  $Re$  when  $Re \geq$   
18  $60$ . This is also observed in K74 for large  $Re$  (their Fig. 14).  $E_c$  from ST73 for  $Re = 97$  is in good  
19 agreement with the curve fit for  $K \sim 1.5$ , but is larger than the curve fit for  $K \sim 0.3$ . It is noteworthy  
20 to explain the shortcomings of these experiments, as mentioned by Pruppacher and Klett (1997).  
21 For the experiment of K74, when  $Re > 100$ , the flow is unsteady and leads to the eddy shedding  
22 and formation of wakes at the top of the particle, which increases the uncertainty in fallspeed. For  
23 the study of ST73, there is an extra problem: the air stream speed was not in agreement with the  
24 fallspeed that the fixed collectors would have, if they were to fall freely.

25 For  $K > 1.0$ , M95 modified the relationship by Langmuir (1948) for  $E_c$  between spherical water  
26 raindrops and cloud droplets, and provided an expression as  $E_c = (K + 1.1)^2 / (K + 1.6)^2$ . However,  
27 this relationship underestimates the best fits to the data of WJ00 (figure not shown). This confirms  
28 the findings of von Blohn et al. (2009) who observed smaller  $E_c$  for raindrops relative to graupel,  
29 and highlights the need for using  $E_c$  for ice particles with realistic shapes and avoiding  $E_c$   
30 surrogates suitable for spherical raindrops.

1 Note that Eqs. (15)-(17) are derived for the range over which the data of WJ00 is valid (e.g.,  $1 <$   
 2  $Re < 120$ ), and they should not be used for extrapolation to  $Re$  values larger or smaller than this  
 3 range. Since  $Re < 1$  corresponds to ice particle smaller than  $D_{thres}$ , it is justified to assume that  $E_c =$   
 4  $0$  in this  $Re$  range. When considering the range  $Re > 120$ , values of  $E_c$  for  $Re = 120$  should be  
 5 used; this is reasonable based on the experiments of K74 for  $200 < Re < 640$ , and the theoretical  
 6 study of WJ00 for  $60 \leq Re \leq 120$ .

7

## 8 5.2 Hexagonal columns

9 H80 and M95 did not provide any  $E_c$  equation for columnar crystals. To the best of our knowledge,  
 10 there is not any practical equation for such crystals in the literature, suitable for use in cloud  
 11 resolving models. In addition to hexagonal plates, WJ00 studied  $E_c$  between hexagonal columns  
 12 (with width  $w$  between 47 and 292.8  $\mu m$ , length  $l$  between 67.1 and 2440  $\mu m$  and  $0.2 < Re < 20$ )  
 13 and water drops of  $1 \mu m < d < 100 \mu m$ . Note that WJ00 calculated  $Re$  for columns in a different  
 14 way than was done for plates.  $Re$  for columns was calculated from their width, whereas  $Re$  for  
 15 plates was computed from  $D$  (e.g.,  $Re_{columns} = wV/\varepsilon$ ). If the values of  $Re$  were calculated from the  
 16 column maximum dimension, they would have values comparable to those for plates. In  
 17 formulating  $E_c$  for columns, we have followed the  $Re$  convention of WJ00. Similar to hexagonal  
 18 plates, we provide the best fits to the data of WJ00 for hexagonal columns:

Deleted: their maximum dimension

$$E_c = \begin{cases} (0.787K^{0.988})(-0.0121Re^2 + 0.1297Re + 0.0598), & 0.01 \leq K \leq K_{thres} \quad \& \quad 0.2 \leq Re \leq 3 \\ (0.787K^{0.988})(-0.0005Re^2 + 0.1028Re + 0.0359), & 0.01 \leq K \leq K_{thres} \quad \& \quad 3 < Re \leq 20 \\ r \sqrt{1 - \frac{1}{3.5} \left[ \log\left(\frac{K}{K_{crit}}\right) - \sqrt{3.5} \right]^2}, & K_{thres} < K < 20 \quad \& \quad 0.2 \leq Re \leq 20 \end{cases} \quad (18)$$

19 where  $K$  is calculated from Eq. (16), and  $K_{crit}$  is calculated as:

$$K_{crit} = \begin{cases} 0.7797 Re^{-0.009}, & 0.2 \leq Re \leq 1.7 \\ 1.0916 Re^{-0.635}, & 1.7 < Re \leq 20 \end{cases} \quad (19)$$

20 and  $r$  is a parameter related to the major radius of the ellipse fit and is determined as:

$$r = \begin{cases} 0.8025 \text{Re}^{0.0604}, & 0.2 \leq \text{Re} \leq 1.7 \\ 0.7422 \text{Re}^{0.2111}, & 1.7 < \text{Re} \leq 20 \end{cases} \quad (20)$$

1 and  $K_{\text{thres}}$  is calculated as:

$$K_{\text{thres}} = \begin{cases} 0.0251 \text{Re}^2 - 0.0144 \text{Re} + 0.811, & 0.2 \leq \text{Re} \leq 2 \\ -0.0003 \text{Re}^3 + 0.0124 \text{Re}^2 - 0.1634 \text{Re} + 1.0075, & 2 < \text{Re} \leq 20 \end{cases} \quad (21)$$

2 The results are shown in Fig. 5b. Similar to hexagonal plates, the curve fits are able to represent  
 3 the data of WJ00 very well over various ranges of  $K$  and  $\text{Re}$ . The percent error in  $E_c$  between the  
 4 curve fits and the WJ00 data has a mean value of 10.28% with a standard deviation of 5.81% for  
 5 all  $\text{Re}$  and  $K$ . There are no experimental estimates of  $E_c$  for hexagonal columns in the literature for  
 6 comparison. For a given  $K$ ,  $E_c$  of columnar ice crystals increases with increasing in  $\text{Re}$  (due to the  
 7 increase in fallspeed). For a given  $\text{Re}$ ,  $E_c$  increases with increasing in  $K$  (because of increasing  
 8 droplet diameter), but it does not exceed 0.95. Unlike plates, the increase in  $\text{Re}$  does not decrease  
 9 the sensitivity of  $E_c$  to  $\text{Re}$ .

10 Again, Eqs. (18)-(21) should not be used for  $\text{Re} < 0.2$  and  $\text{Re} > 20$ . In the range  $\text{Re} < 0.2$ , the  
 11 column size does not exceed the  $D_{\text{thres}}$ , and therefore  $E_c = 0$ . For  $\text{Re} > 20$ , values of  $E_c$  are  
 12 unknown, but we suggest using  $E_c$  for  $\text{Re} = 20$  as a conservative underestimate of  $E_c$ .

13

## 14 6 Mass growth rate by riming

15 In Sect. 4, the dependence of  $\alpha$  on IWC was explained. Unrimed IWC can be derived from  $\alpha$  and  $\beta$   
 16 pertaining to unrimed ice crystals (see EM16). [The riming rate for a single ice particle of size  \$D\$](#) ,  
 17 can be calculated by using the definition of riming mass growth rate, similar to Heymsfield (1982),  
 18 M95 and JH15:

$$\left( \frac{dm}{dt} \right)_{\text{riming}} = \int_0^{d_{\text{max}}} A_g(D, d) |V(D) - v(d)| E(D, d) m(d) n(d) dd \quad (22)$$

19 where  $t$  is time, [d is diameter of a cloud droplet](#),  $A_g(D, d)$  is the geometrical cross-section area of  
 20 the ice particle-cloud droplet collection kernel,  $E(D, d)$  is collection efficiency between the cloud  
 21 droplet and ice particle,  $m(d)$  is the cloud droplet mass,  $n(d)$  is the cloud droplet number

Deleted: R

Deleted: ed

Deleted: IWC

1 distribution, and  $d_{\max}$  is diameter of the largest cloud droplet. Note that the cloud droplet  
2 sedimentation velocity  $v(d)$  is negligible compared to the ice particle fallspeed  $V(D)$  and was  
3 neglected in the similar equation by Heymsfield (1982), M95, and Zhang et al. (2014). Zhang et al.  
4 (2014) used a different equation, which has the form of  $dm/dt = A(D)V(D)E(D)LWC$ , where  
5 LWC is equal to  $\int_0^{d_{\max}} m(d)n(d)dd$ . For this equation, the riming rate is not sensitive to the droplet  
6 distribution.

7 Based on the observations of Locatelli and Hobbs (1974), many cloud and climate models use a  $V$ -  
8  $D$  power law to predict ice mass sedimentation rates ( $V = a_v D^{b_v}$ , with constant  $a_v$  and  $b_v$  for each  
9 specific particle habit; Rutledge and Hobbs, 1984; Ferrier, 1994; Fowler et al., 1996; Pinski et al.,  
10 1998; Morrison and Gettelman, 2008; Gettelman and Morrison, 2015). However, such a  
11 relationship cannot represent the evolution of ice particle size and shape, and is often inconsistent  
12 with the realistic dependence of  $V$  on the ice particle  $m/A$  ratio. This increases uncertainty in the  
13 microphysical and optical properties of such models. To overcome this issue, M96 introduced a  
14 method that derives  $V$  by using  $m$  and  $A$ , and also by a power law for the Best number ( $X$ ) and Re  
15 relationship ( $Re = A_x X^{B_x}$ , where  $A_x$  and  $B_x$  are constant coefficients in specific ranges of  $X$ ). In  
16 this method, the  $V$  calculation depends on the  $m/A$  ratio. Mitchell and Heymsfield (2005) followed  
17 the same method, but they used a  $Re$ - $X$  power law with variable coefficients ( $A$  and  $B$  are not  
18 constant anymore) to produce a smooth transition between different flow regimes. Such an  
19 approach is shown to represent the evolution of  $V$  realistically (MG08; Morrison and Grabowski,  
20 2010; JH15; Morrison and Milbrandt, 2015). In addition, Heymsfield and Westbrook (2010)  
21 developed an alternative method to improve M96 method, and calculated  $X$  as a function of  $m/A_r$   
22 ratio, where  $A_r$  is area ratio (defined as the ratio of ice particle projected area to the projected area  
23 of a circumscribed circle around the particle; see Eq. 15 in Erfani and Mitchell, 2016).

24 Since the contribution of the cloud droplet projected area to  $A_g(D,d)$  is negligible,  $A_g(D,d)$  can be  
25 approximated as the maximum ice particle cross-section area projected normal to the air flow. Ice  
26 particles fall with their major axis perpendicular to the fall direction, therefore  $A_g(D,d)$  is  
27 approximated as the ice particle  $A$ , which is calculated in Sect. 4.2. The  $m(d)$  is calculated from  
28 spherical geometry as:  $m(d) = \pi d^3 \rho_w / 6$ .  $E(D,d)$  is equal to  $E_c E_s$  where  $E_c$  was discussed in  
29 Sect. 5, and  $E_s$  is the sticking efficiency (fraction of the water droplets that stick to the ice particle

Deleted: density

Deleted: is assumed to be zero

1 after collision), and is presumed to be unity since supercooled cloud droplets freeze and bond to an  
 2 ice particle upon collision. Conditions under which  $E_s$  may be less than unity are addressed in  
 3 Pruppacher and Klett (1997). It is noteworthy that by using the above calculations, riming growth  
 4 will be represented in a self-consistent, gradual, and continuous way. Based on the explanations in  
 5 this section, Eq. (22) can be reduced to:

$$\left(\frac{dm}{dt}\right)_{\text{riming}} = A(D)V(D)\int_0^{d_{\text{max}}} E(D,d)m(d)n(d)dd. \quad (23)$$

6 Differentiating Eq. (1) with respect to  $t$  corresponds to  $dm/dt = D^\beta d\alpha/dt + \alpha\beta D^{\beta-1} dD/dt$ , but the  
 7 second term on the RHS should be relatively small (riming has little impact on  $D$  prior to graupel  
 8 formation). Therefore, to a first approximation:

$$\left(\frac{d\alpha}{dt}\right)_{\text{riming}} = \frac{1}{D^\beta} \left(\frac{dm}{dt}\right)_{\text{riming}}, \quad (24)$$

9 and together with Eq. (23), a change in  $\alpha$  due to riming can be determined. *Since  $D$  and  $\beta$  do not*  
 10 *change by riming,  $d\alpha/dt$  is linearly proportional to  $dm/dt$ .*

11 Figure 6 shows  $dm/dt$  calculated from Eq. (23) for hexagonal ice plates *and hexagonal columns* for  
 12 different values of LWC and droplet median-mass diameter (MMD; the droplet diameter that  
 13 divides the droplet PSD mass into equal parts).  $E_c$  is calculated from Eqs. (15) *and (18) for*  
 14 *hexagonal plates and hexagonal columns, respectively*, and a sub-exponential PSD is assumed for  
 15 cloud droplets that has the form:

$$n(d) = N_o d^\nu \exp(-\lambda d), \quad (25)$$

16 where  $\lambda$  is the PSD slope parameter,  $\nu$  is the PSD dispersion parameter and  $N_o$  is intercept  
 17 parameter. M95 used observational droplet spectra from Storm Peak lab (Steamboat [Springs](#),  
 18 Colorado, USA), and calculated various PSD parameters:  $\nu = 9$ ,  $\lambda = (\nu + 1)/\bar{d}$ , and  
 19  $N_o = 4 \times 10^4 LWC / \rho_w \bar{d}^{13}$ , where  $\bar{d}$  is droplet mean diameter, and is related to MMD as  
 20  $MMD = 1.26\bar{d}$  for this dataset. Note that all variables are in units of cgs. It is seen in Fig. 6a that  
 21  $dm/dt$  [for riming](#) increases with increasing ice particle  $D$ . The  $dm/dt$  is linearly proportional to  
 22 LWC when MMD and  $D$  are constant. In addition, when LWC is constant, doubling MMD (from 8  
 23 to 16  $\mu\text{m}$ ) leads to a quadrupling of  $dm/dt$ . One important feature is the contribution of small

Formatted: Font:Italic, Complex Script Font: Italic

1 droplets ( $d < 10 \mu\text{m}$ ) to  $dm/dt$ , when  $K < 0.7$  and  $E_c < 0.3$ . It is seen in this figure that when MMD  
 2 is relatively small ( $= 8 \mu\text{m}$ ), ignoring such small droplets results in values of  $(dm/dt)_{\text{riming}}$  at the  
 3 largest crystal sizes that are  $\sim 40\%$  (for plates) and  $\sim 70\%$  (for columns) of those obtained when all  
 4 droplets are included. That is, small droplets contribute about 60% and 30%, respectively, to the  
 5  $(dm/dt)_{\text{riming}}$  values at the largest sizes. This surprising contribution from small droplets is partly  
 6 due to half of the LWC being associated with  $d < 8 \mu\text{m}$ . However, when MMD is larger ( $= 16 \mu\text{m}$ ),  
 7 the contribution from small droplets is only  $\sim 5\%$ . The size-dependence of  $dm/dt$  for hexagonal  
 8 columns (Fig. 6b) shows that  $dm/dt$  for columns is larger than that for hexagonal plates for a  
 9 specific crystal size when droplet MMD is  $8 \mu\text{m}$ , partly because columns fall faster than plates (see  
 10 Fig. 6 in M96) and partly due to higher  $E_c$  for columns encountering larger droplets. Moreover,  
 11 when LWC is constant, doubling MMD (from 8 to  $16 \mu\text{m}$ ) leads to at least a doubling of  $dm/dt$   
 12 (greater for plates).

13 The collection kernel ( $K_c$ ) can be calculated as  $A(D)V(D)E(D,d)$ , which is alternatively equal to  
 14  $dm/dt$  divided by the ice particle mass due to riming (see Eq. 23). MG08 approximated this  
 15 variable by using simple assumptions, and found that it is proportional to  $D^2$ . Here, we showed by  
 16 more accurate analysis that  $K_c$  has a form of a second-order polynomial fit, and is represented for  
 17 MMD =  $8 \mu\text{m}$  by  $K_c = 7 \times 10^{-6} D^2 - 0.0002D + 0.0008$ .

## 19 7 Conclusions

20 In most atmospheric models, riming is treated as an abrupt change between precipitation classes;  
 21 from snow to graupel, which occurs at an arbitrary threshold size. Such parameterizations are not  
 22 realistic and lead to uncertainty in the simulation of snowfall. In this study, a combination of  
 23 various empirical and theoretical approaches is utilized to shed light on the riming process. SCPP  
 24 ground-based measurements of  $m$  and  $D$  for rimed and unrimed ice particles are used in this study;  
 25 such particles represent ice clouds for  $-40 \text{ }^\circ\text{C} < T < 0 \text{ }^\circ\text{C}$ . The findings presented here suggest a  
 26 fundamental shift in our way of representing ice particle mass and projected area in atmospheric  
 27 models for riming. It is common in most models to assume that riming increases  $\beta$  (Eq. 1) from  
 28 values of  $\sim 2$  (for dendrites) to values of  $\sim 3$  (for graupel). However, we showed that this  
 29 assumption is not supported by observations. To a good approximation under most conditions,  
 30 riming does not increase (or decrease)  $\beta$  and  $D$  in an  $m$ - $D$  power law and the treatment of riming is

Formatted: Subscript

Deleted: 0.2

Deleted: 35

Formatted: Font:Italic

Formatted: Font:Italic, Subscript

Deleted: effect of

Deleted: LWC

Deleted: Pattern of  $dm/dt$  for hexagonal columns (Fig. 6b) shows that  $dm/dt$  for columns is larger than that for plates for a specific size, because columns fall faster than plates (see Fig. 6 in M96). Moreover, when LWC is constant, doubling MMD (from 8 to  $16 \mu\text{m}$ ) leads to a doubling of  $dm/dt$ . The contribution of small droplets to  $dm/dt$  is less than that for hexagonal plates. When MMD is equal to  $8 \mu\text{m}$ , ignoring the small droplets results in values of  $dm/dt$  at the largest crystal sizes that are  $\sim 70\%$  of those obtained when all droplets are included. The reason for this difference between hexagonal columns and plates is that values of  $E_c$  for columns-small drops are larger than that for plates-small drops (See Fig. 5). For columns,  $E_c$  does not exceed 0.3 for  $K < 0.2$  ( $d < 5 \mu\text{m}$ ), whereas for plates,  $d$  can reach to  $10 \mu\text{m}$  before  $E_c$  exceeds 0.3.

Formatted: Font:(Default) +Theme Headings CS (Times New Roman), 12 pt, Complex Script Font: +Theme Headings CS (Times New Roman), 12 pt

Formatted: Justified

Formatted: Font:(Default) +Theme Headings CS (Times New Roman), 12 pt, Italic, Complex Script Font: +Theme Headings CS (Times New Roman), 12 pt, Italic

Formatted: Font:(Default) +Theme Headings CS (Times New Roman), 12 pt, Complex Script Font: +Theme Headings CS (Times New Roman), 12 pt

Formatted: Font:Italic, Complex Script Font: Italic

Formatted: Font:(Default) +Theme Headings CS (Times New Roman), 12 pt, Complex Script Font: +Theme Headings CS (Times New Roman), 12 pt

Deleted:  $m$

Deleted:  $A$

1 simplified with riming increasing only  $\alpha$  during the phase 1 of riming (before the formation of  
 2 graupel). To represent unrimed particles in frontal clouds, one could enlist the polynomial fit for  
 3 synoptic ice clouds ( $-40^{\circ}\text{C} < T < -20^{\circ}\text{C}$ , see EM16) but adjust this equation to conform to the  
 4 observed power laws for unrimed dendrites. To treat riming for dendrites, this fit equation could be  
 5 multiplied by the riming fraction  $m_r/m_u$  or alternatively  $\text{IWC}/\text{IWC}_u$ . A similar strategy could be  
 6 adopted for other ice particle shapes or shape mixtures in frontal clouds, as is done for columnar  
 7 particles in this study. By using this method, there is no discontinuity in the growth of  $m$  and  $A$ ;  
 8 rather, the particles grow gradually during riming process. Phase 2 of riming starts when graupel  
 9 with quasi-spherical shape forms. In this phase, the increase in  $m$  and  $A$  causes an increase in  $D$ .  
 10 It is straightforward for models with multiple ice categories to utilize our new method. This can be  
 11 done by describing riming growth as two phases and removing the autoconversion process. Phase  
 12 1 simulates the growth from ice crystal to the onset of graupel formation. In this phase, mass and  
 13 projected area gradually increase, but size is unchanged (Eqs. 6-11). Phase 2 represents graupel  
 14 growth. In this phase, the shape is unchanged, but mass, projected area, and size gradually increase  
 15 (Eqs. 12-14). Prior to this work, there was no practical method to calculate  $E_c$  in models explicitly  
 16 for columnar crystals. Moreover, most models use the H80 equation to calculate  $E_c$  for planar  
 17 crystals, but this equation has important drawbacks inherited from the early numerical studies (See  
 18 Sect. 1.2). To solve this problem, new equations for the calculation of  $E_c$  are developed based on  
 19 the numerical study of WJ00 for both hexagonal plates and hexagonal columns that accounts for  
 20 dependence of  $E_c$  on cloud droplet  $d$  and ice particle  $D$  in non-steady flow. In the future, this  
 21 treatment of the riming process will be employed in a new snow growth model that predicts the  
 22 vertical evolution of ice particle size spectra, mass, projected area, fallspeed, and snowfall rate in  
 23 terms of the growth processes of vapor diffusion, aggregation and riming. These results will be  
 24 compared with airborne measurements from two spiral descents.

Formatted: Font:Italic, Complex Script Font: Italic  
 Formatted: Font:Italic, Complex Script Font: Italic  
 Formatted: Font:Italic, Complex Script Font: Italic

Deleted: adding  
 Deleted: transitional  
 Deleted: after ice crystal phase,  
 Deleted: of particle  
 Deleted: graupel  
 Deleted: the additional  
 Deleted: of graupel  
 Deleted: -  
 Deleted: T  
 Deleted: i

Deleted: SGM

Deleted: a

26 **Appendix A: List of symbols and their definitions**

27  $a_v$  prefactor in fall speed-dimension power law

28  $A$  projected area

29  $A_g$  geometrical cross-section area

- 1  $A_{\max}$  graupel projected area
- 2  $A_r$  projected area ratio
- 3  $A_y$  prefactor in Reynolds number-Best number power law
- 4  $b_v$  exponent in fall speed-dimension power law
- 5  $B_x$  exponent in Reynolds number-Best number power law
- 6  $d$  water drop diameter
- 7  $\bar{d}$  drop mean diameter
- 8  $D$  maximum dimension of ice particle
- 9  $D_g$  maximum dimension of initial graupel (at the end of phase 1 of riming)
- 10  $E$  collection efficiency
- 11  $E_c$  collision efficiency
- 12  $E_s$  sticking efficiency
- 13  $g$  gravitational constant
- 14  $k$  correction factor for graupel projected area
- 15  $K$  mixed Froude number
- 16  $K_{crit}$  critical value of mixed Froude number
- 17  $K_c$  collection kernel
- 18  $K_{thres}$  threshold of  $K$
- 19  $l$  length of columnar crystals
- 20  $m$  mass of ice particle
- 21  $m_r$  rimed mass
- 22  $m_u$  unrimed mass
- 23  $m_{\max}$  graupel mass
- 24  $m_{\text{mix}}$  mass of mixture of rimed and unrimed particles
- 25  $M_f$  ice mass flux
- 26  $n$  number density
- 27  $N_o$  intercept parameter of a gamma PSD

- 1  $P$  air pressure
- 2  $r$  parameter related to the major radius of the ellipse fit
- 3  $Re$  Reynolds number
- 4  $t$  time
- 5  $T$  temperature
- 6  $v$  terminal fall speed of water drop
- 7  $V$  terminal fallspeed of ice particle
- 8  $V_g$  volume of initial graupel (at the end of phase 1 of riming)
- 9  $V_m$  mass-weighted terminal fallspeed
- 10  $w$  width of columnar crystals
- 11  $X$  Best number
- 12  $\alpha$  prefactor in mass-dimension power law
- 13  $\beta$  exponent in mass-dimension power law
- 14  $\gamma$  prefactor in projected area-dimension power law
- 15  $\delta$  exponent in projected area-dimension power law
- 16  $\varepsilon$  kinematic viscosity
- 17  $\mu$  dynamic viscosity
- 18  $\lambda$  slope parameter of a gamma PSD
- 19  $\nu$  dispersion parameter of a gamma PSD
- 20  $\rho_a$  air density
- 21  $\rho_g$  initial graupel bulk density (at the end of phase 1 of riming)
- 22  $\rho_i$  ice density
- 23  $\rho_w$  water density

24 **Acknowledgements**

25 This research was supported by the Office of Science (BER), U.S. Department of Energy. We are  
26 grateful to Brad Baker for providing us with the measurements of ice particle projected area that  
27 were used in BL06. We are also thankful of two anonymous reviewers for their constructive

Deleted: -

1 [comments that improve the paper](#). The SCPP data used in this study and associated software is  
2 freely available to interested researchers; those interested should contact the second author.

3

#### 4 References

- 5 [Avramov, A., Ackerman, A. S., Fridlind, A. M., van Dierenhoven, B., Botta, G., Aydin, K., Verlinde, J., Korolev, A. V., Strapp, J. W., McFarquhar, G. M., Jackson, R., Brooks, S. D., Glen, A., and Wolde, M.: Toward ice formation closure in Arctic mixed-phase boundary layer clouds during ISDAC, \*J. Geophys. Res.\*, 116, 2011.](#)
- 6
- 7 [Baker, B. and Lawson, R. P.: Improvement in determination of ice water content from two-dimensional particle imagery. Part I: Image-to-mass relationships, \*J. Appl. Meteorol. & Clim.\*, 45, 1282-1290, 2006.](#)
- 8
- 9 [Beard, K. V. and Grover, S. N.: Numerical Collision Efficiencies for Small Raindrops Colliding with Micron Size Particles, \*J. Atmos. Sci.\*, 31, 543-550, 1974.](#)
- 10
- 11 [Brientjes, R. T., Heymsfield, A. J., and Krauss, T. W.: Examination of double-plate ice crystals and the initiation of precipitation in continental cumulus clouds, \*J. Atmos. Sci.\*, 44, 1331-1349, 1987.](#)
- 12
- 13 [Cotton, R. J., Field, P. R., Ulanowski, Z., Kaye, P. H., Hirst, E., Greenaway, R. S., Crawford, I., Crosier, J., and Dorsey, J.: The effective density of small ice particles obtained from in situ aircraft observations of mid-latitude cirrus, \*Q. J. Roy. Meteor. Soc.\*, 139, 1923-1934, 2013.](#)
- 14
- 15 [Eidhammer, T., Morrison, H., Banesmer, A., Gettelman, A., and Heymsfield, A. J.: Comparison of ice cloud properties simulated by the Community Atmosphere Model \(CAM5\) with in-situ observations, \*Atmos. Chem. Phys.\*, 14, 10103-10118, 2014.](#)
- 16
- 17 [Erfani, E. and Mitchell, D. L.: Developing and bounding ice particle mass- and area-dimension expressions for use in atmospheric models and remote sensing, \*Atmos. Chem. Phys.\*, 16, 4379-4400, 2016.](#)
- 18
- 19 [Feng, D. and Grant, L.: Correlation of snow crystal habit, number flux and snowfall intensity from ground observations, \*Conf. on Cloud Physics, Amer. Meteor. Soc., Boston, Massachusetts\*, 485-487, 1982.](#)
- 20
- 21 [Ferrier, B. S.: A Double-Moment Multiple-Phase Four-Class Bulk Ice Scheme. Part I: Description, \*J. Atmos. Sci.\*, 51, 249-280, 1994.](#)
- 22
- 23 [Fontaine, E., Schwarzenboeck, A., Delanoe, J., Wobrock, W., Leroy, D., Dupuy, R., Gourbeyre, C., and Protat, A.: Constraining mass-diameter relations from hydrometeor images and cloud radar reflectivities in tropical continental and oceanic convective anvils, \*Atmos. Chem. Phys.\*, 14, 11367-11392, 2014.](#)
- 24
- 25 [Fowler, L. D., Randall, D. A., and Rutledge, S. A.: Liquid and ice cloud microphysics in the CSU general circulation model. I. Model description and simulated microphysical processes, \*J. Clim.\*, 9, 489-529, 1996.](#)
- 26
- 27 [Fukuta, N. and Takahashi, T.: The growth of atmospheric ice crystals: A summary of findings in vertical supercooled cloud tunnel studies, \*J. Atmos. Sci.\*, 56, 1963-1979, 1999.](#)
- 28
- 29 [Gettelman, A. and Morrison, H.: Advanced Two-Moment Bulk Microphysics for Global Models. Part I: Off-Line Tests and Comparison with Other Schemes, \*J. Clim.\*, 28, 1268-1287, 2015.](#)
- 30
- 31 [Hall, W. D.: A Detailed Microphysical Model Within a Two-Dimensional Dynamic Framework: Model Description and Preliminary Results, \*J. Atmos. Sci.\*, 37, 2486-2507, 1980.](#)
- 32
- 33
- 34
- 35
- 36

**Deleted:** Avramov, A., Ackerman, A. S., Fridlind, A. M., van Dierenhoven, B., Botta, G., Aydin, K., Verlinde, J., Korolev, A. V., Strapp, J. W., McFarquhar, G. M., Jackson, R., Brooks, S. D., Glen, A., and Wolde, M.: Toward ice formation closure in Arctic mixed-phase boundary layer clouds during ISDAC, *J. Geophys. Res.*, 116, 2011. - [1]

**Formatted:** Indent: Before: 0", Hanging: 0.19", Space After: 0 pt, Line spacing: 1.5 lines

1 [Harimaya, T.: Riming properties of snow crystals, J. Meteor. Soc. Japan, 53, 384-392, 1975.](#)

2 [Harimaya, T. and Sato, M.: Measurement of the riming amount on snowflakes, J. Fac. Sci., Hokkaido Univ., 8, 355-](#)

3 [366, 1989.](#)

4 [Heymsfield, A. J.: A Comparative Study of the Rates of Development of Potential Graupel and Hail Embryos in High](#)

5 [Plains Storms, J. Atmos. Sci., 39, 2867-2897, 1982.](#)

6 [Heymsfield, A. J.: Characteristics of graupel particles in northeastern Colorado cumulus congestus clouds, J. Atmos.](#)

7 [Sci., Boston, 35, 284-295, 1978.](#)

8 [Heymsfield, A. J. and Miloshevich, L. M.: Homogeneous Ice Nucleation and Supercooled Liquid Water in Orographic](#)

9 [Wave Clouds, J. Atmos. Sci., 50, 2335-2353, 1993.](#)

10 [Heymsfield, A. J., Schmitt, C., Bansemer, A., and Twohy, C. H.: Improved Representation of Ice Particle Masses](#)

11 [Based on Observations in Natural Clouds, J. Atmos. Sci., 67, 3303-3318, 2010.](#)

12 [Heymsfield, A. J. and Westbrook, C. D.: Advances in the Estimation of Ice Particle Fall Speeds Using Laboratory and](#)

13 [Field Measurements, J. Atmos. Sci., 67, 2469-2482, 2010.](#)

14 [Hobbs, P. V.: Organization and structure of clouds and precipitation on the mesoscale and microscale in cyclonic](#)

15 [storms, Rev. of Geophys. Space Phys., 16, 741-755, 1978.](#)

16 [Jensen, A. A. and Harrington, J. Y.: Modeling Ice Crystal Aspect Ratio Evolution during Riming: A Single-Particle](#)

17 [Growth Model, J. Atmos. Sci., 72, 2569-2590, 2015.](#)

18 [Kajikawa, M.: On the collection efficiency of snow crystals for cloud droplets, J. Meteor. Soc. Japan, 52, 328-336,](#)

19 [1974.](#)

20 [Kalesse, H., Szyrmer, W., Kneifel, S., Kollias, P., and Luke, E.: Fingerprints of a riming event on cloud radar Doppler](#)

21 [spectra: observations and modeling, Atmos. Chem. Phys., 16, 2997-3012, 2016.](#)

22 [Khain, A., Pokrovsky, A., and Sednev, I.: Some effects of cloud-aerosol interaction on cloud microphysics structure](#)

23 [and precipitation formation: numerical experiments with a spectral microphysics cloud ensemble model, Atmos.](#)

24 [Res., 52, 195-220, 1999.](#)

25 [Langmuir, I.: The production of rain by a chain reaction in cumulus clouds at temperatures above freezing, J.](#)

26 [Meteorol., 5, 175-192, 1948.](#)

27 [Locatelli, J. d. and Hobbs, P. V.: Fall speeds and masses of solid precipitation particles, J. Geophys. Res., 79, 2185-](#)

28 [2197, 1974.](#)

29 [Magono, C. and Lee, C. W.: Meteorological Classification of Natural Snow Crystals, J. Fac. Sci., Hokkaido](#)

30 [University., Ser. 7, 2, No. 4., 1966.](#)

31 [Matejka, T. J., Houze, R. A., and Hobbs, P. V.: Microphysics and dynamics of clouds associated with mesoscale](#)

32 [rainbands in extratropical cyclones, Quart. J. R. Met. Soc., 106, 29-56, 1980.](#)

33 [Mitchell, D. L.: An analytical model predicting the evolution of ice particle size distributions, PhD, University of](#)

34 [Nevada-Reno, PhD Dissertation, 181 pp., 1995.](#)

35 [Mitchell, D. L.: Evolution of snow-size spectra in cyclonic storms .I. snow growth by vapor-deposition and](#)

36 [aggregation, J. Atmos. Sci., 45, 3431-3452, 1988.](#)

1 [Mitchell, D. L.: Use of mass- and area-dimensional power laws for determining precipitation particle terminal](#)  
2 [velocities, J. Atmos. Sci., 53, 1710-1723, 1996.](#)

3 [Mitchell, D. L. and d'Entremont, R. P.: Satellite retrieval of the liquid water fraction in tropical clouds between -20](#)  
4 [and -38 °C, Atmos. Meas. Tech., 5, 1683-1698, 2012.](#)

5 [Mitchell, D. L. and Erfani, E.: Developing and bounding ice particle mass- and area-dimension expressions for use in](#)  
6 [climate models and remote sensing Boston, MA2014.](#)

7 [Mitchell, D. L. and Heymsfield, A. J.: Refinements in the treatment of ice particle terminal velocities, highlighting](#)  
8 [aggregates, J. Atmos. Sci., 62, 1637-1644, 2005.](#)

9 [Mitchell, D. L., Huggins, A., and Grubisic, V.: A new snow growth model with application to radar precipitation](#)  
10 [estimates, Atmos. Res., 82, 2-18, 2006.](#)

11 [Mitchell, D. L., Zhang, R., and Pitter, R. L.: Mass-dimensional relationships for ice particles and the influence of](#)  
12 [riming on snowfall rates, J. Appl. Meteorol., 29, 153-163, 1990.](#)

13 [Morrison, H. and Gettelman, A.: A new two-moment bulk stratiform cloud microphysics scheme in the community](#)  
14 [atmosphere model, version 3 \(CAM3\). Part I: Description and numerical tests, J. Clim., 21, 3642-3659, 2008.](#)

15 [Morrison, H. and Grabowski, W. W.: A novel approach for representing ice microphysics in models: Description and](#)  
16 [tests using a kinematic framework, J. Atmos. Sci., 65, 1528-1548, 2008.](#)

17 [Morrison, H. and Grabowski, W. W.: An Improved Representation of Rimed Snow and Conversion to Graupel in a](#)  
18 [Multicomponent Bin Microphysics Scheme, J. Atmos. Sci., 67, 1337-1360, 2010.](#)

19 [Morrison, H. and Milbrandt, J. A.: Parameterization of Cloud Microphysics Based on the Prediction of Bulk Ice](#)  
20 [Particle Properties. Part I: Scheme Description and Idealized Tests, J. Atmos. Sci., 72, 287-311, 2015.](#)

21 [Murakami, M., Kikuchi, K., and Magono, C.: Experiments on aerosol scavenging by natural snow crystals.](#)  
22 [Part I: Collection efficiencies of uncharged snow crystals for micron and submicron particles., J. Meteorol. Soc.](#)  
23 [Japan, 63, 119-129, 1985.](#)

24 [Pflaum, J. C. and Pruppacher, H. R.: A Wind Tunnel Investigation of the Growth of Graupel Initiated from Frozen](#)  
25 [Drops, J. Atmos. Sci., 36, 680-689, 1979.](#)

26 [Pinsky, M., Khain, A., Rosenfeld, D., and Pokrovsky, A.: Comparison of collision velocity differences of drops and](#)  
27 [graupel particles in a very turbulent cloud, Atmos. Res., 49, 99-113, 1998.](#)

28 [Pitter, R. L.: A reexamination of riming on thin ice plates, J. Atmos. Sci., 34, 684-685, 1977.](#)

29 [Pitter, R. L. and Pruppacher, H. R.: A numerical investigation of collision efficiencies of simple ice plates colliding](#)  
30 [with supercooled water drops J. Atmos. Sci., 31, 551-559, 1974.](#)

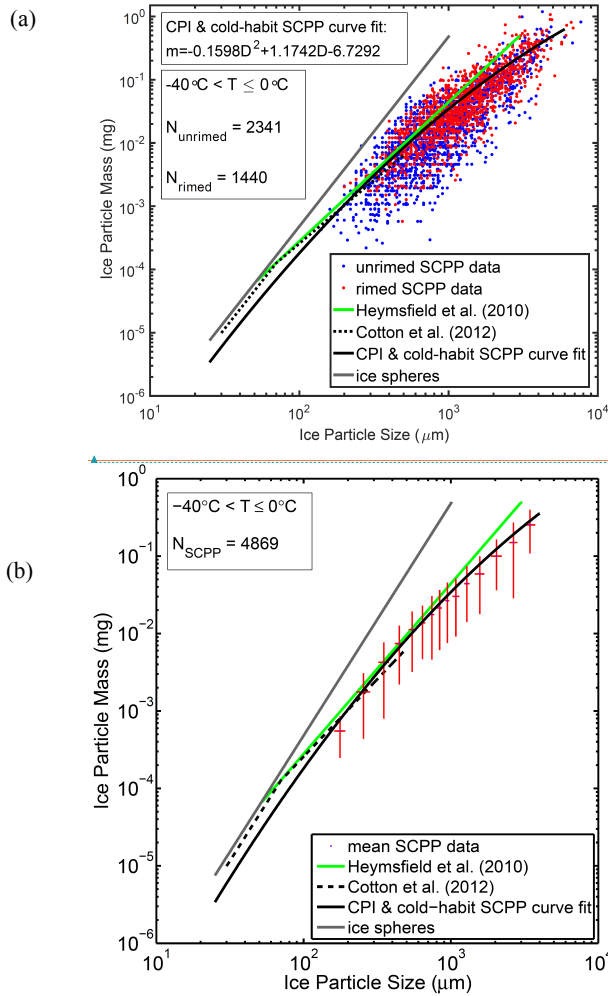
31 [Pruppacher, H. R. and Klett, J. D.: Microphysics of clouds and precipitation: 2nd edn, Kluwer Academic Publishers,](#)  
32 [Dordrecht, the Netherlands, 1997.](#)

33 [Rasmussen, R. M. and Heymsfield, A. J.: A Generalized Form for Impact Velocities Used to Determine Graupel](#)  
34 [Accretional Densities, J. Atmos. Sci., 42, 2275-2279, 1985.](#)

35 [Reisin, T., Levin, Z., and Tzivion, S.: Rain production in convective clouds as simulated in an axisymmetric model](#)  
36 [with detailed microphysics. I. Description of the model, J. Atmos. Sci., 53, 497-519, 1996.](#)

1 [Rogers, D. C.: Aggregation of natural ice crystals, Wyoming Univ., Laramie. Dept. of Atmospheric Resources,](#)  
2 [Report AR110, 35-35, 1974.](#)  
3 [Rosenfeld, D. and Woodley, W. L.: Deep convective clouds with sustained supercooled liquid water down to -37.5](#)  
4 [degrees C, Nature, 405, 440-442, 2000.](#)  
5 [Rutledge, S. A. and Hobbs, P. V.: The Mesoscale and Microscale Structure and Organization of Clouds and](#)  
6 [Precipitation in Midlatitude Cyclones. XII: A Diagnostic Modeling Study of Precipitation Development in Narrow](#)  
7 [Cold-Frontal Rainbands, J. Atmos. Sci., 41, 2949-2972, 1984.](#)  
8 [Sasyo, Y. and Tokue, H.: The Collection Efficiency of Simulated Snow Particles for Water Droplets \(Preliminary](#)  
9 [Report\), Pap. Meteor. Geophys., 24, 1-12, 1973.](#)  
10 [Schlamp, R. J., Pruppacher, H. R., and Hamielec, A. E.: A Numerical Investigation of the Efficiency with which](#)  
11 [Simple Columnar Ice Crystals Collide with Supercooled Water Drops, J. Atmos. Sci., 32, 2330-2337, 1975.](#)  
12 [Shupe, M. D., Matrosov, S. Y., and Uttal, T.: Arctic mixed-phase cloud properties derived from surface-based sensors](#)  
13 [at SHEBA, J. Atmos. Sci., 63, 697-711, 2006.](#)  
14 [Takahashi, T. and Fukuta, N.: Supercooled Cloud Tunnel Studies on the Growth of Snow Crystals between -4 and -](#)  
15 [20 °C, J. Meteor. Soc. Japan, 66, 841-855, 1988.](#)  
16 [von Blohn, N., Diehl, K., Mitra, S. K., and Bormann, S.: Riming of Graupel: Wind Tunnel Investigations of](#)  
17 [Collection Kernels and Growth Regimes, J. Atmos. Sci., 66, 2359-2366, 2009.](#)  
18 [Wang, P. K. and Ji, W. S.: Collision efficiencies of ice crystals at low-intermediate Reynolds numbers colliding with](#)  
19 [supercooled cloud droplets: A numerical study, J. Atmos. Sci., 57, 1001-1009, 2000.](#)  
20 [Zhang, D., Wang, Z., Heymsfield, A., Fan, J., and Luo, T.: Ice Concentration Retrieval in Stratiform Mixed-Phase](#)  
21 [Clouds Using Cloud Radar Reflectivity Measurements and 1D Ice Growth Model Simulations, J. Atmos. Sci., 71,](#)  
22 [3613-3635, 2014.](#)



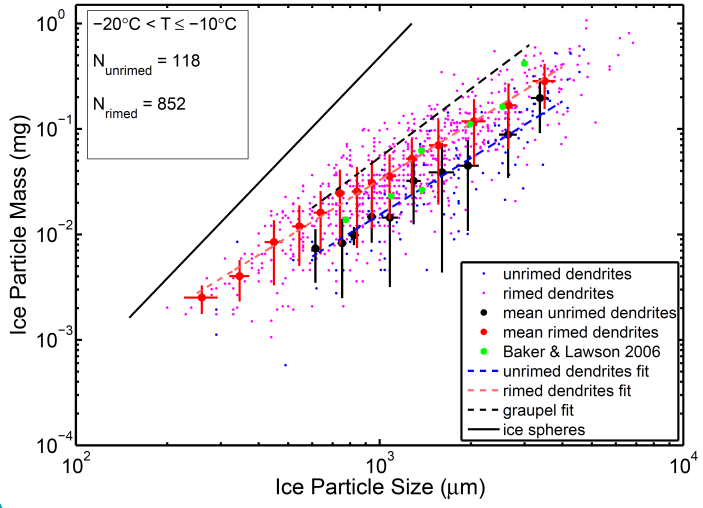


1

2  
3

4 Figure 1. (a) Comparing the m-D curve fit based on the CPI and cold-habit SCPP data (EM16) with SCPP ice particle  
5 m-D measurements corresponding to all classifiable shapes. Unrimed and rimed particles are indicated by blue and red  
6 dots, respectively. m-D power laws from two other studies are also displayed. (b) Similar to (a), except that all the  
7 SCPP data (including unclassifiable ice particles) have been grouped into size-bins; mean (red cross-intersection  
8 points) and standard deviation (red bars) in each size-bin are shown.

1



Formatted: Font:(Default) +Theme Headings CS (Times New Roman), 12 pt, Complex Script Font: +Theme Headings CS (Times New Roman), 12 pt

2

3

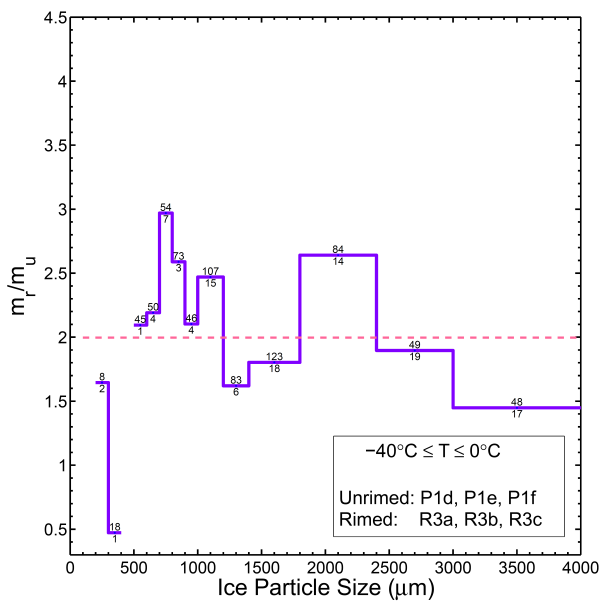
4

5

6

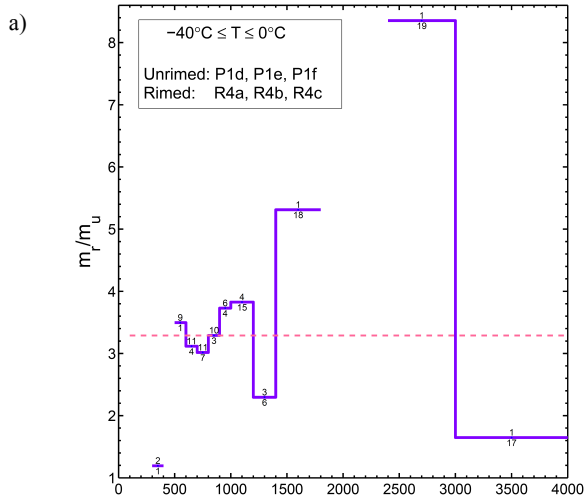
7

Figure 2. Ice particle m-D measurements corresponding to rimed (pink dots) and unrimed (blue dots) dendrites using SCPP data. Mean (circles) and standard deviations (bars) in each size bin are also displayed for both rimed (red) and unrimed (black) dendrites. Green filled circles indicate dendrites from BL06.

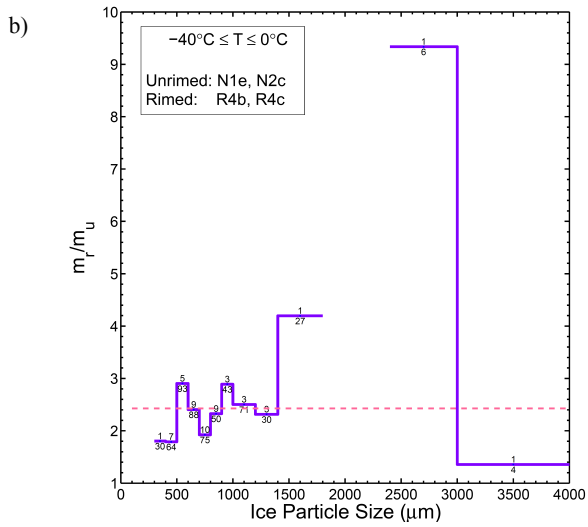


1  
 2 Figure 3. Rimed-to-unrimed mass ratio  $m_r/m_u$  (violet lines) for each common size-bin in Figure 2, based on heavily  
 3 rimed and unrimed dendrites. The pink line indicates the weighted mean of  $m_r/m_u$ . The numbers on the top (bottom) of  
 4 each violet line shows the number of rimed (unrimed) particles in that size bin.  
 5

1

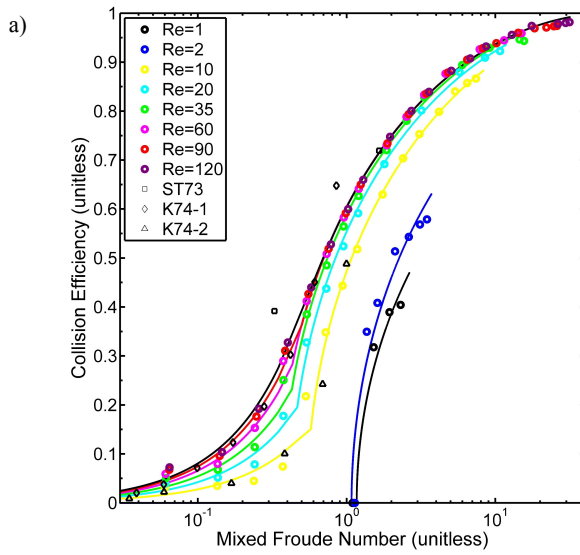


2

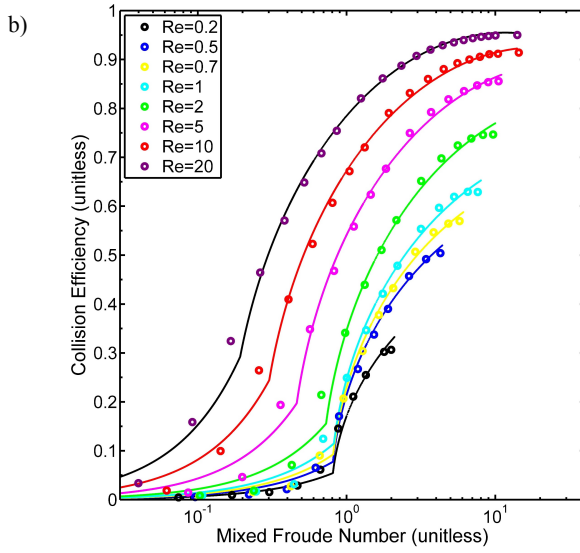


3

4 Figure 4. (a) Same as Fig. 3, but rimed particles are now graupel. (b) Same as (a), but unrimed particles are now  
5 columnar crystals and R4a (hexagonal graupel) is not included.



1



2

3

4

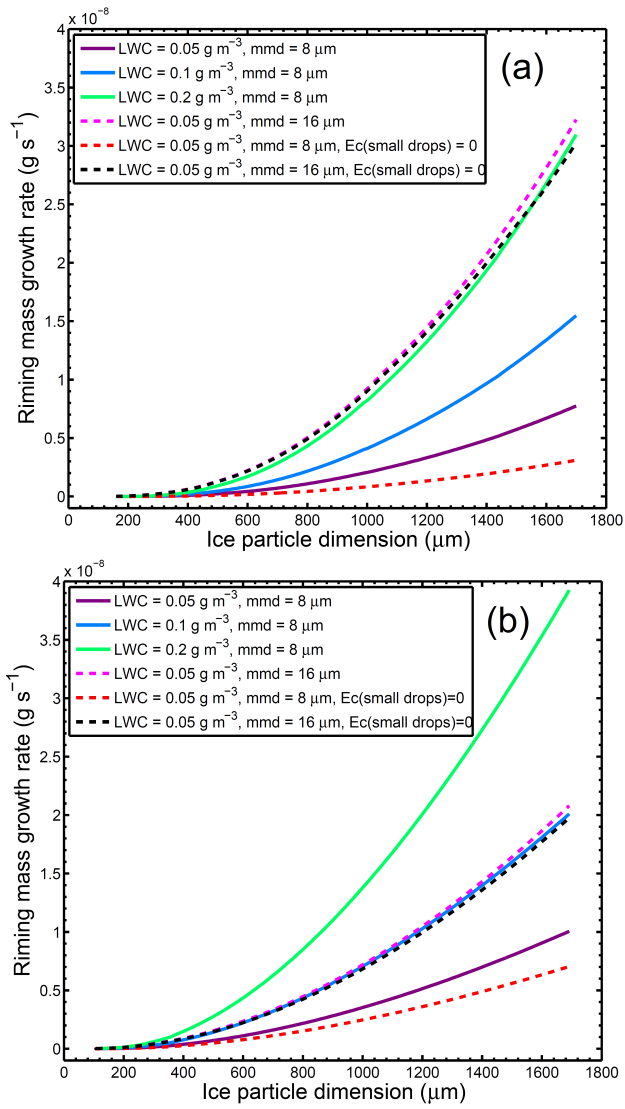
5

6

7

8

Figure 5. (a) Collision efficiency for hexagonal plates as a function of the mixed Froude number. Circles show the data of WJ00 based on numerical calculations, and curves show the best fits to this data for various values of Re. Also displayed are experimental data of ST73 for Re = 97 (squares), K74 for  $200 \leq \text{Re} \leq 640$  (diamonds), and K74 for  $10 \leq \text{Re} \leq 35$  (triangles). (b) Same as (a), but for hexagonal columns and no experimental data.



1  
2  
3 Figure 6. Riming mass growth rate versus ice particle maximum dimension,  $D$  for various LWC ( $0.05, 0.1$  and  $0.2 g$   
4  $m^{-3}$ ) and different droplet median-mass diameters ( $8$  and  $16 \mu m$ ) for (a) hexagonal plates and (b) hexagonal columns.  
5 Additional curves (dashed red and dashed black curves) are produced by assuming that  $E_c$  conforms to the ellipse  
6 model and is zero for smaller droplets.

Deleted: hexagonal plate

- Avramov, A., Ackerman, A. S., Fridlind, A. M., van Diedenoven, B., Botta, G., Aydin, K., Verlinde, J., Korolev, A. V., Strapp, J. W., McFarquhar, G. M., Jackson, R., Brooks, S. D., Glen, A., and Wolde, M.: Toward ice formation closure in Arctic mixed-phase boundary layer clouds during ISDAC, *J. Geophys. Res.*, 116, 2011.
- Baker, B. and Lawson, R. P.: Improvement in determination of ice water content from two-dimensional particle imagery. Part I: Image-to-mass relationships, *J. Appl. Meteorol. & Clim.*, 45, 1282-1290, 2006.
- Beard, K. V. and Grover, S. N.: Numerical Collision Efficiencies for Small Raindrops Colliding with Micron Size Particles, *J. Atmos. Sci.*, 31, 543-550, 1974.
- Bruintjes, R. T., Heymsfield, A. J., and Krauss, T. W.: Examination of double-plate ice crystals and the initiation of precipitation in continental cumulus clouds, *J. Atmos. Sci.*, 44, 1331-1349, 1987.
- Cotton, R. J., Field, P. R., Ulanowski, Z., Kaye, P. H., Hirst, E., Greenaway, R. S., Crawford, I., Crosier, J., and Dorsey, J.: The effective density of small ice particles obtained from in situ aircraft observations of mid-latitude cirrus, *Q. J. Roy. Meteor. Soc.*, 139, 1923-1934, 2013.
- Eidhammer, T., Morrison, H., Bansemer, A., Gettelman, A., and Heymsfield, A. J.: Comparison of ice cloud properties simulated by the Community Atmosphere Model (CAM5) with in-situ observations, *Atmos. Chem. Phys.*, 14, 10103-10118, 2014.
- Erfani, E. and Mitchell, D. L.: Developing and bounding ice particle mass- and area-dimension expressions for use in atmospheric models and remote sensing, *Atmos. Chem. Phys.*, 16, 4379-4400, doi:10.5194/acp-16-4379-2016, 2016.
- Feng, D. and Grant, L.: Correlation of snow crystal habit, number flux and snowfall intensity from ground observations, *Conf. on Cloud Physics*, Amer. Meteor. Soc., Boston, Massachusetts, 485-487, 1982.
- Ferrier, B. S.: A Double-Moment Multiple-Phase Four-Class Bulk Ice Scheme. Part I: Description, *J. Atmos. Sci.*, 51, 249-280, 1994.
- Fontaine, E., Schwarzenboeck, A., Delanoe, J., Wobrock, W., Leroy, D., Dupuy, R., Gourbeyre, C., and Protat, A.: Constraining mass-diameter relations from hydrometeor images and cloud radar reflectivities in tropical continental and oceanic convective anvils, *Atmos. Chem. Phys.*, 14, 11367-11392, 2014.
- Fowler, L. D., Randall, D. A., and Rutledge, S. A.: Liquid and ice cloud microphysics in the CSU general circulation model .1. Model description and simulated microphysical processes, *J. Clim.*, 9, 489-529, 1996.
- Fukuta, N. and Takahashi, T.: The growth of atmospheric ice crystals: A summary of findings in vertical supercooled cloud tunnel studies, *J. Atmos. Sci.*, 56, 1963-1979, 1999.
- Gettelman, A. and Morrison, H.: Advanced Two-Moment Bulk Microphysics for Global Models. Part I: Off-Line Tests and Comparison with Other Schemes, *J. Clim.*, 28, 1268-1287, 2015.
- Hall, W. D.: A Detailed Microphysical Model Within a Two-Dimensional Dynamic Framework: Model Description

- and Preliminary Results, *J. Atmos. Sci.*, 37, 2486-2507, 1980.
- Harimaya, T.: Riming properties of snow crystals, *J. Meteor. Soc. Japan*, 53, 384-392, 1975.
- Harimaya, T. and Sato, M.: Measurement of the riming amount on snowflakes, *J. Fac. Sci., Hokkaido Univ.*, 8, 355-366, 1989.
- Heymsfield, A. J.: A Comparative Study of the Rates of Development of Potential Graupel and Hail Embryos in High Plains Storms, *J. Atmos. Sci.*, 39, 2867-2897, 1982.
- Heymsfield, A. J.: Characteristics of graupel particles in northeastern Colorado cumulus congestus clouds, *J. Atmos. Sci.*, Boston. 35, 284-295, 1978.
- Heymsfield, A. J. and Miloshevich, L. M.: Homogeneous Ice Nucleation and Supercooled Liquid Water in Orographic Wave Clouds, *J. Atmos. Sci.*, 50, 2335-2353, 1993.
- Heymsfield, A. J., Schmitt, C., Bansemer, A., and Twohy, C. H.: Improved Representation of Ice Particle Masses Based on Observations in Natural Clouds, *J. Atmos. Sci.*, 67, 3303-3318, 2010.
- Hobbs, P. V.: Organization and structure of clouds and precipitation on the mesoscale and microscale in cyclonic storms, *Rev. of Geophys. Space Phys.*, 16, 741-755, 1978.
- Jensen, A. A. and Harrington, J. Y.: Modeling Ice Crystal Aspect Ratio Evolution during Riming: A Single-Particle Growth Model, *J. Atmos. Sci.*, 72, 2569-2590, 2015.
- Kajikawa, M.: On the collection efficiency of snow crystals for cloud droplets, *J. Meteor. Soc. Japan*, 52 328-336, 1974.
- Kalesse, H., Szyrmer, W., Kneifel, S., Kollias, P., and Luke, E.: Fingerprints of a riming event on cloud radar Doppler spectra: observations and modeling, *Atmos. Chem. Phys.*, 16, 2997-3012, 2016.
- Khain, A., Pokrovsky, A., and Sednev, I.: Some effects of cloud-aerosol interaction on cloud microphysics structure and precipitation formation: numerical experiments with a spectral microphysics cloud ensemble model, *Atmos. Res.*, 52, 195-220, 1999.
- Langmuir, I.: The production of rain by a chain reaction in cumulus clouds at temperatures above freezing, *J. Meteorol.*, 5, 175-192, 1948.
- Locatelli, J. d. and Hobbs, P. V.: Fall speeds and masses of solid precipitation particles, *J. Geophys. Res.*, 79, 2185-2197, 1974.
- Matejka, T. J., Houze, R. A., and Hobbs, P. V.: Microphysics and dynamics of clouds associated with mesoscale rainbands in extratropical cyclones, *Quart. J. R. Met. Soc.*, 106, 29-56, 1980.
- Mitchell, D. L.: An analytical model predicting the evolution of ice particle size distributions, PhD, University of Nevada-Reno, PhD Dissertation, 181 pp., 1995.
- Mitchell, D. L.: Use of mass- and area-dimensional power laws for determining precipitation particle terminal

- velocities, *J. Atmos. Sci.*, 53, 1710-1723, 1996.
- Mitchell, D. L. and d'Entremont, R. P.: Satellite retrieval of the liquid water fraction in tropical clouds between -20 and -38 °C, *Atmos. Meas. Tech.*, 5, 1683-1698, 2012.
- Mitchell, D. L. and Erfani, E.: Developing and bounding ice particle mass- and area-dimension expressions for use in climate models and remote sensing Boston, MA2014.
- Mitchell, D. L. and Heymsfield, A. J.: Refinements in the treatment of ice particle terminal velocities, highlighting aggregates, *J. Atmos. Sci.*, 62, 1637-1644, 2005.
- Mitchell, D. L., Huggins, A., and Grubisic, V.: A new snow growth model with application to radar precipitation estimates, *Atmos. Res.*, 82, 2-18, 2006.
- Mitchell, D. L., Zhang, R., and Pitter, R. L.: Mass-dimensional relationships for ice particles and the influence of riming on snowfall rates, *J. Appl. Meteorol.*, 29, 153-163, 1990.
- Morrison, H. and Gettelman, A.: A new two-moment bulk stratiform cloud microphysics scheme in the community atmosphere model, version 3 (CAM3). Part I: Description and numerical tests, *J. Clim.*, 21, 3642-3659, 2008.
- Morrison, H. and Grabowski, W. W.: A novel approach for representing ice microphysics in models: Description and tests using a kinematic framework, *J. Atmos. Sci.*, 65, 1528-1548, 2008.
- Morrison, H. and Grabowski, W. W.: An Improved Representation of Rimed Snow and Conversion to Graupel in a Multicomponent Bin Microphysics Scheme, *J. Atmos. Sci.*, 67, 1337-1360, 2010.
- Morrison, H. and Milbrandt, J. A.: Parameterization of Cloud Microphysics Based on the Prediction of Bulk Ice Particle Properties. Part I: Scheme Description and Idealized Tests, *J. Atmos. Sci.*, 72, 287-311, 2015.
- Murakami, M., Kikuchi, K., and Magono, C.: Experiments on aerosol scavenging by natural snow crystals. Part I: Collection efficiencies of uncharged snow crystals for micron and submicron particles., *J. Meteorol. Soc. Japan*, 63, 119-129, 1985.
- Pflaum, J. C. and Pruppacher, H. R.: A Wind Tunnel Investigation of the Growth of Graupel Initiated from Frozen Drops, *J. Atmos. Sci.*, 36, 680-689, 1979.
- Pinsky, M., Khain, A., Rosenfeld, D., and Pokrovsky, A.: Comparison of collision velocity differences of drops and graupel particles in a very turbulent cloud, *Atmos. Res.*, 49, 99-113, 1998.
- Pitter, R. L.: A reexamination of riming on thin ice plates, *J. Atmos. Sci.*, 34, 684-685, 1977.
- Pitter, R. L. and Pruppacher, H. R.: A numerical investigation of collision efficiencies of simple ice plates colliding with supercooled water drops *J. Atmos. Sci.*, 31, 551-559, 1974.
- Pruppacher, H. R. and Klett, J. D.: *Microphysics of clouds and precipitation: 2nd edn*, Kluwer Academic Publishers, Dordrecht, the Netherlands, 1997.
- Rasmussen, R. M. and Heymsfield, A. J.: A Generalized Form for Impact Velocities Used to Determine Graupel

- Accretional Densities, *J. Atmos. Sci.*, 42, 2275-2279, 1985.
- Reisin, T., Levin, Z., and Tzivion, S.: Rain production in convective clouds as simulated in an axisymmetric model with detailed microphysics .1. Description of the model, *J. Atmos. Sci.*, 53, 497-519, 1996.
- Rogers, D. C.: Aggregation of natural ice crystals, Wyoming Univ., Laramie. Dept. of Atmospheric Resources, Report AR110, 35-35, 1974.
- Rosenfeld, D. and Woodley, W. L.: Deep convective clouds with sustained supercooled liquid water down to -37.5 degrees C, *Nature*, 405, 440-442, 2000.
- Rutledge, S. A. and Hobbs, P. V.: The Mesoscale and Microscale Structure and Organization of Clouds and Precipitation in Midlatitude Cyclones. XII: A Diagnostic Modeling Study of Precipitation Development in Narrow Cold-Frontal Rainbands, *J. Atmos. Sci.*, 41, 2949-2972, 1984.
- Sasyo, Y. and Tokue, H.: The Collection Efficiency of Simulated Snow Particles for Water Droplets (Preliminary Report), *Pap. Meteor. Geophys.*, 24, 1-12, 1973.
- Schlamp, R. J., Pruppacher, H. R., and Hamielec, A. E.: A Numerical Investigation of the Efficiency with which Simple Columnar Ice Crystals Collide with Supercooled Water Drops, *J. Atmos. Sci.*, 32, 2330-2337, 1975.
- Shupe, M. D., Matrosov, S. Y., and Uttal, T.: Arctic mixed-phase cloud properties derived from surface-based sensors at SHEBA, *J. Atmos. Sci.*, 63, 697-711, 2006.
- Takahashi, T. and Fukuta, N.: Supercooled Cloud Tunnel Studies on the Growth of Snow Crystals between -4 and -20 °C, *J. Meteor. Soc. Japan*, 66, 841-855, 1988.
- von Blohn, N., Diehl, K., Mitra, S. K., and Borrmann, S.: Riming of Graupel: Wind Tunnel Investigations of Collection Kernels and Growth Regimes, *J. Atmos. Sci.*, 66, 2359-2366, 2009.
- Wang, P. K. and Ji, W. S.: Collision efficiencies of ice crystals at low-intermediate Reynolds numbers colliding with supercooled cloud droplets: A numerical study, *J. Atmos. Sci.*, 57, 1001-1009, 2000.
- Zhang, D., Wang, Z., Heymsfield, A., Fan, J., and Luo, T.: Ice Concentration Retrieval in Stratiform Mixed-Phase Clouds Using Cloud Radar Reflectivity Measurements and 1D Ice Growth Model Simulations, *J. Atmos. Sci.*, 71, 3613-3635, 2014.